IEEE Access
Multidisciplinary | Rapid Review | Open Access Journal

Received September 11, 2018, accepted October 8, 2018, date of publication October 17, 2018,
date of current version November 19, 2018.

Digital Object Identifier 10.1109/ACCESS.2018.2876496

Design and Testing of a Nonlinear Model Predictive Controller for Ride Height Control of Automotive Semi-Active Air Suspension Systems

XINBO MA[1], PAK KIN WONG[1], JING ZHAO[1], JIAN-HUA ZHONG[2], HUANG YING[1], AND XING XU[3]

[1]Department of Electromechanical Engineering, University of Macau, Taipa 999078, Macau
[2]School of Mechanical and Automation Engineering, Fuzhou University, Fuzhou 350108, China
[3]School of Automotive and Traffic Engineering, Jiangsu University, Zhenjiang 212013, China

Corresponding author: Jian-Hua Zhong (jhzhong@fzu.edu.cn)

This work was supported in part by the research grant of the University of Macau under Grant MYRG2016-00212-FST and Grant MYRG2017-00135-FST, in part by the National Natural Science Foundation of China under Grant 51875105, Grant 51375013, and Grant 51705084, and in part by the Youth Teacher Educational Research Fund of the Fujian Provincial Education Office under Grant JAT170090.

ABSTRACT With the rapid growth of the automotive technology, electronically controlled air suspension has been widely used to improve ride comfort and handling stability of the vehicle by actively modulating the suspension stiffness, vehicle height, and posture. Ride height control (RHC) is the main function of the semi-active air suspension, and it is achieved by conducting air charging and discharging of the air spring, which plays a critical role in improving the vehicle dynamic performance. In addition, the unevenness distribution with payloads at the four wheels, the different dynamic characteristics of the front and rear air suspensions, and the undesired roll and pitch angles make adjustment effect of the vehicle ride height hard to be well addressed. Therefore, an effective control strategy is very essential, which is not only for RHC but also for keeping the vehicle posture, as well as the vehicle dynamic performance. Considering that the full car dynamics is a highly nonlinear model, this paper proposes a novel nonlinear model predictive controller to handle the multi-objective control requirement of a full car system. In order to evaluate the performance of the proposed controller, comparisons among the proposed control algorithm, the existing proportional–integral–derivative method, and the sliding-mode controller are carried out by a numerical analysis. The numerical results show that the proposed method excels the other methods and is effective in the adjustment of the vehicle ride height.

INDEX TERMS Air suspension, nonlinear model predictive controller, multi-objective control, ride height control.

I. INTRODUCTION

In recent years, the air suspension system has been widely employed in the commercial vehicle for its superiority in improving the vehicle dynamics [1]–[3] and simplicity on ride height control (RHC) [4]–[6]. The air suspension system is regarded as an air-operated, microprocessor controlled suspension system and the RHC function is achieved by charging and discharging the air to the air spring via the pneumatic circuit connected to the air spring. A large number of investigations have been done on the control of the air suspension system in order to fully explore the performance of the RHC system [6]–[10].

Basically, the air suspension system is a kind of semi-active suspension (SAS) system [11], [12], and several algorithms have been proposed for the control of the SAS system [13]–[17]. Some of the representative algorithms, such as the proportional-integral-derivative (PID) control [16], [18], H infinity control [19], sliding mode control (SMC) [10], [20] have attracted numerous attention due to their feasibilities of improving the vehicle dynamics in both academia and industry.

Though PID method offers the simplest and yet the most efficient solution to most real-world control problems, it is still hard to get a perfect balance among the three gains which have an impact on the steady-state and transient response of the control system [21]. The designed PID gains may not resist the uncertainties and disturbances if the parameters of the vehicle system cannot be estimated precisely or achieved;

hence the PID controller has low robustness. Furthermore, it is a tedious work to adjust the PID gains, which means that its parameters are difficult to be adjusted with the variable vehicle status.

As for the H infinity algorithm, it is a kind of robust control strategy and can achieve stabilization with guaranteed performance [19]. The robust control techniques have more advantages than classical control techniques. They are readily applicable to multivariate systems with cross-coupling problems. However, the basic concept of robust control techniques is to use massive control variables so that the controlled plant could reach convergence. This requirement of the controller leads to chattering which causes limited system precision and significant wear on the driving mechanism. Moreover, because the control system generally does not work in the optimal state with the control method, the accuracy of the control system is poor when it is at steady-state.

Additionally, SMC is a nonlinear control method which could alter the dynamics of the nonlinear system by applying a discontinuous control signal. SMC can switch from one continuous structure to the other based on the current position with state space [22]. Furthermore, it is characterized by the robust and rapid response, insensitivity to parameter variations and external disturbances, order reduction and so on. Nevertheless, SMC is a non-smooth controller so that the state trajectory goes through the sliding mode surface back and forth. Thus chattering will be generated when the state trajectory reaches the sliding mode surface. The constant chattering from the controller will definitely cause the instability of the vehicle, which is basically divergent to the purpose of the control scheme.

Particularly, there are several challenges for RHC with the SAS system: the high complexity of the control system owing to the control of four air springs simultaneously; the significant vertical oscillations of the vehicle sprung mass caused by the nonlinearity of the air compressibility; the undesired roll and pitch angles of the vehicle body inevitably raised during the RHC process. In view of the limitations of the aforesaid control methods and the nonlinear nature of the semi-active air suspension (SAAS) system, a nonlinear model predictive controller (NMPC) is proposed in this study.

Generally, NMPC is designed for the control of nonlinear systems, which is subject to input and state constraints and multi-objective control problems. The NMPC is an optimization design for the feedback control of the nonlinear system and its primary applications are stabilization and tracking problems. The benefits of the NMPC can be easily summarized as follows: (1) The multiple objectives can be formulated in a unified multi-variable framework of the NMPC; (2) The constructed multi-variable system with NMPC method can be easily accessed and adjusted by the designer; (3) The constraints of the multi-variable system that preset by the designer can be tuned within a wide range; (4) The simplicity of the constructed multi-variable system can lead to a fast response with less computational time [23]. Hence, one objective of this project is to design a NMPC for RHC of the SAAS system, so that an optimal result can be obtained.

Compared with the above-mentioned methods, NMPC is able to bring the control variable to its set-point quickly, smoothly and without steady-state offset. Moreover, NMPC deals with constraints explicitly without any degradation in the quality of control. Also, NMPC also demonstrates superior performance in the presence of a moderate amount of error for the model parameters, and the process is brought to its set-point without steady-state offset [24]–[27].

Since the core of NMPC is the prediction model, the modeling of the adjustable air spring with the SAAS system should be fully understood. It is well-known that the model of the SAAS system includes severe nonlinearities, the stiffness of the air spring and hysteresis characteristics of the air spring. Recently, some researches have been carried out to develop an analytical air spring model. In 2006, an air spring model with SAAS system was developed to express both stiffness and hysteresis of the air spring [28]. Considering the nonlinear characteristics of air variation and the contoured piston of air springs, a new dynamic model for air springs was introduced in [29]. Moreover, [30] derived a nonlinear model of an air spring by assuming adiabatic or isothermal conditions and analyzed the stiffness with the derived model.

However, most of the existing studies on air springs assume that the air pressure in the working process keeps constant, which means that the thermodynamic effect of air on the air spring dynamic characteristic is neglected. Although [30] presented an air spring model that is expressed as a function of air pressure, volume, effective area, and the polytropic index. The pressure of the air spring is analyzed without consideration of thermodynamics. Additionally, [29] developed a pre-charged air spring model by thermodynamics. However, the air charging and discharging processes of the air spring were not considered in the developed model. As a result, another objective of this project is to develop an exact analytical air spring model which considers the pressure variation based on thermodynamics and can predict the dynamic characteristics of the SAAS system accurately. As more conditions are considered in the model, it is believed that the model developed will be highly nonlinear.

According to the requirement of NMPC design, the basic step is to linearize the proposed nonlinear model and turn it into linear state-space form, in which the nonlinear control problem is transformed into a linear model control problem. Then, the optimal control signal can be obtained by the NMPC. At this point, one of the research objectives is to linearize the proposed nonlinear model for the SAAS system. The main novelties of this paper can be summarized as follows: (1) It is a novel work to develop an analytical nonlinear model of the SAAS system which considers the time-varying air pressure during working process; (2) The linearization of the vehicle model for the NMPC design is a pioneering work;

(3) A new multi-objective NMPC method is designed, which aims to regulate not only the vehicle ride height, but also the roll and pitch angles of the vehicle body. With the proposed NMPC, the overall vehicle performance, including the ride quality, the road holding and the handling capacities, will be further improved.

The rest of this paper is organized as follows: Section 2 proposes the air spring model of SAAS at first. Then, the model with full car system and its linearization method are introduced. Section 3 presents the design process of the NMPC. Simulations with analysis are illustrated in Section 4. Finally, Conclusions of the research are given in Section 5.

II. PROBLEM FORMULATION AND MODELING

To effectively achieve the goal of ride height and posture control, it is necessary to gain a thorough understanding of the full car dynamic system. Therefore, it is critical to derive an analytical nonlinear model of a general full car, which can reflect the changes of the bounce, the roll and pitch angles of the vehicle body. In this Section, the dynamic behaviors of the air spring during the vehicle height and posture adjustment process is completed first. Then, the nonlinear model of the vehicle height and posture adjustment system is built. This section is mainly composed of mathematical expressions for the air spring, full car model with the air suspension system and road excitation of the four wheels. Finally, some reasonable linear approximations for components nonlinearities are proposed, so that the nonlinear model predictive controller for the vehicle height and posture adjustment system can be successfully designed.

A. DSCRIPTION OF SEMI-ACTIVE AIR SPRING SUSPENSION SYSTEM

Electronically controlled air spring (ECAS) not only can achieve modulation of vehicle height during driving via conducting gas charging and discharging of the air spring but also prevent the unstable phenomenon of the vehicle posture which caused by the uneven vehicle payload distribution and the different system parameters between the front air suspension and the rear air suspension. A schematic diagram for the vehicle height adjustment of a full car is provided in Figure 1. The system is composed of the ECAS and the air charging and discharging (ACD) system.

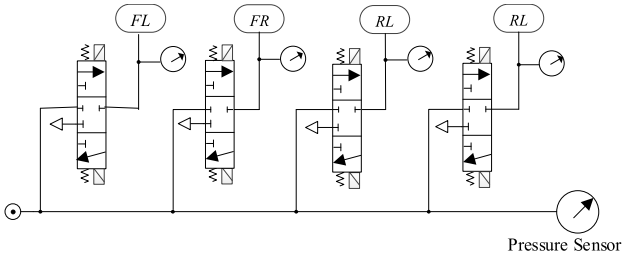

FIGURE 1. 2-DOF vehicle model with ECAS and ACD system.

According to the principle of this system, the lifting and lowering procedures of the RHC and posture control are as follows,

Leveling Up Procedure: When the vehicle height needs to be leveled, the air pressure in the air tank is smaller than that in the air spring. Therefore, the compressor starts to supply high-pressure air to the air tank. Then, the compressed air flows from the air tank to the air spring. Meanwhile, undesirably asynchronous height adjustment at the four corners of the vehicle may be emerged during the leveling up process, which leads to unduly large pitch and roll angles. As a result, the unstable phenomenon of the vehicle posture is emerged. Hence, it is necessary to control the ride height of the four corners synchronously.

Lowering Down Procedure: When the vehicle height needs to be lowered, the air in the air spring needs to be discharged to the atmosphere, thus the volume of the air spring decreases and then the vehicle height drops. During the lowering down procedure, the control strategy for the unstable phenomenon of the vehicle posture is similar to the leveling up procedure.

B. NONLINEAR MODEL OF FULL CAR WITH SAAS SYSTEM

An analytical nonlinear model of the RHC system for the full car is typically derived for controller design and simulation test. The modeling work starts with the modeling of the air spring.

1) AIR SPRING MODELING

The following assumptions are made to develop the mathematical model of the air spring.

1. The compressor block and the reservoir tank are simplified to a high-pressure source, and atmospheric environment is regarded as a low-pressure source.
2. The air is a perfect gas, and its kinetic energy is negligible in all air springs.
3. The temperature of the air is homogeneous in all air springs.
4. There is no mass flow leakage in the system components.
5. The cross-sectional area of the air spring is constant.
6. The dynamics of unsprung mass of the vehicle is neglected.
7. The gas process, which defines the relationship between pressure and specific volume in the air spring, is given by the polytrophic relationship, where κ is the polytropic index and K is the polytropic process constant

$$pv^{\kappa} = K \tag{1}$$

8. The solenoid valve is modeled by a static area-normalized mass flow equation while ignoring the dynamic property, as shown in Equation (2), where Cq is the flow coefficient, k is the specific heat ratio for air, p_u is the upstream pressure and p_d is the downstream pressure. The flow type depends on the pressure ratio

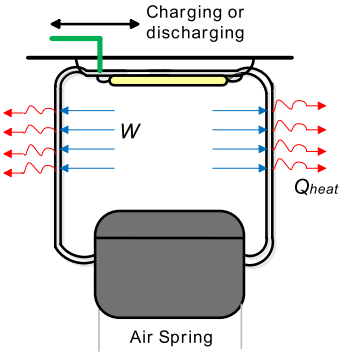

FIGURE 2. Energy flow behavior of air spring [31].

(p_d/p_u) and the critical pressure ratio P_{cr} which is defined as $P_{cr} = \left(\frac{2}{k+1}\right)^{\frac{k}{k-1}}$ [31].

$$q(p_u, p_{dn}) = \begin{cases} \sqrt{\frac{2k}{R(k-1)}}\sqrt{\left(\frac{p_d}{p_u}\right)^{\frac{2}{k}} - \left(\frac{p_d}{p_u}\right)^{\frac{k+1}{k}}}\frac{C_q p_u}{\sqrt{T}}, \\ \quad \text{if } \left(\frac{p_d}{p_u}\right) \geq P_{cr}\ (unchoked) \\ \sqrt{\frac{k}{R}\left(\frac{2}{k+1}\right)^{\frac{k+1}{k-1}}}\frac{C_q p_u}{\sqrt{T}}, \\ \quad \text{if } \left(\frac{p_d}{p_u}\right) < P_{cr}\ (choked) \end{cases} \tag{2}$$

Then, the following simplified adjustable air spring is obtained. Due to the differential temperature between the inner and outer sides of the control volume, a heat transfer will be generated in theory. In order to establish the model of the air spring during the ride height control process, the mathematical expression of the air spring during the gas charging and discharging processes is derived based on thermodynamic theory [31]. Figure 2 shows the energy flow behavior of the air spring.

$$\dot{Q}_{heat} + \dot{W} + h_{in}q_{in} - h_{out}q_{out} = \dot{U}_{as} \tag{3}$$

where $\dot{Q}_{heat}$ is the heat transfer rate between the inner and the outer sides of the control volume, W denotes the power that is performed on the control volume. The specific enthalpy of the air flowing into and outside the control volume is h_{in} and h_{out}, respectively. q_{in} is the air mass flow to the air spring, q_{out} is the air mass flow exiting from the air spring. U_{as} is the internal energy of the air spring control volume.

The duration of ride height and posture adjustment is relatively short, and there is not enough time for heat transfer during the process. Hence, the heat transfer between the inside and outside of the air spring can be neglected. Meantime, the power that is performed on the control volume W is defined as,

$$\dot{W} = -p_{as}\dot{V}_{as} \tag{4}$$

where p_{as} is the air pressure of the air spring and V_{as} is the volume of the air spring.

The internal energy of the air spring control volume U_{as} is defined by the specific heat at constant volume c_v, the temperature inside the control volume of the air spring T, and the air mass inside the air spring m_{as} and is given by,

$$\dot{U}_{as} = c_v d\left(Tm_{as}\right)/dt \tag{5}$$

According to the ideal gas equation of state $p_{as}V_{as} = m_{as}RT$, the internal energy of the air spring control volume can be obtained as,

$$\dot{U}_{as} = (c_v/R)\left[d\left(p_{as}V_{as}\right)/dt\right] = (c_v/R)\left(p_{as}\dot{V}_{as} + V_{as}\dot{p}_{as}\right) \tag{6}$$

where R is the perfect gas constant.

Moreover, the specific enthalpy of the air flowing into and outside the air spring are expressed using the specific heat at constant pressure c_p and the air temperature T,

$$h_{in} = h_{out} = c_p T \tag{7}$$

Therefore, the equation of energy flow for the air in the air spring can be obtained from Eq. (3)$\sim$ Eq. (7),

$$(c_v/R)\left(p_{as}\dot{V}_{as} + V_{as}\dot{p}_{as}\right) = -p_{as}\dot{V}_{as} + c_p T\left(q_{in} - q_{out}\right) \tag{8}$$

The relationship between the specific heat at constant pressure and the specific heat at constant volume is expressed as follows,

$$c_p/c_v = \kappa, \quad c_p - c_v = R \tag{9}$$

where κ is the polytropic index.

The model of the air spring during the ride height adjustment process can be obtained as,

$$V_{as}\dot{p}_{as} = \kappa RT\left(q_{in} - q_{out}\right) - \kappa p_{as}\dot{V}_{as} \tag{10}$$

The parameters V_{as} and $\dot{V}_{as}$ can be expressed by the following equations,

$$V_{as} = A_{as}\left(z_{as0} + z_{as}\right), \quad \dot{V}_{as} = A_{as}\dot{z}_{as} \tag{11}$$

$$z_{as} = z_s - z_{us}, \quad \dot{z}_{as} = \dot{z}_s - \dot{z}_{us} \tag{12}$$

where A_{as} is the air spring cross-sectional area, z_{as0} is the initial air spring displacement, z_{as} is the air spring displacement. z_s and z_{us} are the bounce of the vehicle and unsprung mass displacement, respectively.

Hence, the model of the air spring can be finally expressed as,

$$\dot{p}_{as}A_{as}\left(z_{as0} + z_s - z_{us}\right) = \kappa RT\left(q_{in} - q_{out}\right) - \kappa p_{as}A_{as}\left(\dot{z}_s - \dot{z}_{us}\right) \tag{13}$$

2) FULL CAR MODEL WITH ACTIVE AIR SUSPENSION SYSTM

The full car dynamic model with SAAS system is shown in Figure 3.

Based on the Newton's law and vehicle dynamics, the full car dynamic model with the SAAS system can be formulated

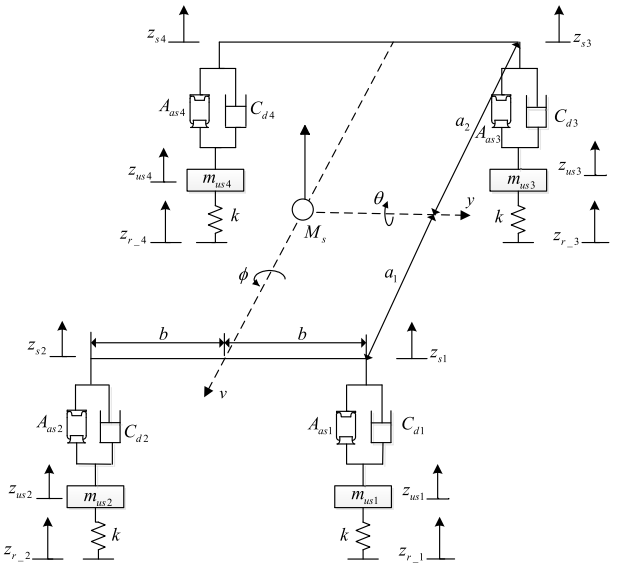

FIGURE 3. Full car dynamic model.

as follows [32],

$$\begin{cases} M_s\ddot{z}_s = p_{as1}A_{as1} + p_{as2}A_{as2} + p_{as3}A_{as3} + p_{as4}A_{as4} \\ \quad -C_{d1}\left(\dot{z}_{s1} - \dot{z}_{us1}\right) - C_{d2}\left(\dot{z}_{s2}\right. \\ \quad \left. - \dot{z}_{us2}\right) - C_{d3}\left(\dot{z}_{s3} - \dot{z}_{us3}\right) - C_{d4}\left(\dot{z}_{s4} - \dot{z}_{us4}\right) \\ I_v\ddot{\phi} = bp_{as1}A_{as1} - bp_{as2}A_{as2} + bp_{as3}A_{as3} - p_{as4}A_{as4} \\ \quad -bC_{d1}\left(\dot{z}_{s1} - \dot{z}_{us1}\right) + bC_{d2}\left(\dot{z}_{s2} - \dot{z}_{us2}\right) \\ \quad -bC_{d3}\left(\dot{z}_{s3} - \dot{z}_{us3}\right) + bC_{d4}\left(\dot{z}_{s4} - \dot{z}_{us4}\right) \\ I_y\ddot{\theta} = a_1p_{as1}A_{as1} + a_1p_{as2}A_{as2} - a_2p_{as3}A_{as3} - a_2p_{as4}A_{as4} \\ \quad -a_1C_{d1}\left(\dot{z}_{s1} - \dot{z}_{us1}\right) - a_1C_{d2}\left(\dot{z}_{s2} - \dot{z}_{us2}\right) \\ \quad +a_2C_{d3}\left(\dot{z}_{s3} - \dot{z}_{us3}\right) + a_2C_{d4}\left(\dot{z}_{s4} - \dot{z}_{us4}\right) \\ m_{us1}\ddot{z}_{us1} = k\left(z_{r\_1} - z_{us1}\right) - p_{as1}A_{as1} + C_{d1}\left(\dot{z}_{s1} - \dot{z}_{us1}\right) \\ m_{us2}\ddot{z}_{us2} = k\left(z_{r\_2} - z_{us2}\right) - p_{as2}A_{as2} + C_{d2}\left(\dot{z}_{s2} - \dot{z}_{us2}\right) \\ m_{us3}\ddot{z}_{us3} = k\left(z_{r\_3} - z_{us3}\right) - p_{as3}A_{as3} + C_{d3}\left(\dot{z}_{s3} - \dot{z}_{us3}\right) \\ m_{us4}\ddot{z}_{us4} = k\left(z_{r\_4} - z_{us4}\right) - p_{as4}A_{as4} + C_{d4}\left(\dot{z}_{s4} - \dot{z}_{us4}\right) \end{cases} \tag{14}$$

where z_s is the bounce of the vehicle body, ϕ and θ are the roll angle and pitch angle of vehicle body, respectively? M_s is the vehicle body mass, I_v and I_y are the moment of inertia around the v-axis and moment of inertia around the y-axis, respectively. m_{usi} $(i = 1, 2, 3, 4)$ is the unsprung mass of the i^{th} corner of the vehicle, z_{usi} $(i = 1, 2, 3, 4)$ is the unsprung mass displacement, z_{si} $(i = 1, 2, 3, 4)$ is the sprung mass displacement, z_{r_i} $(i = 1, 2, 3, 4)$ is the road roughness of the i^{th} corner. a_1 and a_2 are the distance from the center of gravity to the front wheel and rear wheel, respectively. b is the half-track width, k is the coefficient of tire stiffness. A_{asi} $(i = 1, 2, 3, 4)$ is the cross-sectional area of each air spring, p_{asi} $(i = 1, 2, 3, 4)$ is the air spring pressure and C_{di} $(i = 1, 2, 3, 4)$ is the damping coefficient.

Moreover, the model of the air spring, which reflects the change of pressure in the control volume and the vertical displacement during the ride height and posture adjustment, can be obtained as follows,

$$\begin{cases} \dot{p}_{as1}A_{as1}\left(z_{as0\_1} + z_{s1} - z_{us1}\right) = \kappa RT\left(q_{in\_1} - q_{out\_1}\right) \\ \quad -\kappa p_{as1}A_{as1}\left(\dot{z}_{s1} - \dot{z}_{us1}\right) \\ \dot{p}_{as2}A_{as2}\left(z_{as0\_2} + z_{s2} - z_{us2}\right) = \kappa RT\left(q_{in\_2} - q_{out\_2}\right) \\ \quad -\kappa p_{as2}A_{as2}\left(\dot{z}_{s2} - \dot{z}_{us2}\right) \\ \dot{p}_{as3}A_{as3}\left(z_{as0\_3} + z_{s3} - z_{us3}\right) = \kappa RT\left(q_{in\_3} - q_{out\_3}\right) \\ \quad -\kappa p_{as3}A_{as3}\left(\dot{z}_{s3} - \dot{z}_{us3}\right) \\ \dot{p}_{as4}A_{as4}\left(z_{as0\_4} + z_{s4} - z_{us4}\right) = \kappa RT\left(q_{in\_4} - q_{out\_4}\right) \\ \quad -\kappa p_{as4}A_{as4}\left(\dot{z}_{s4} - \dot{z}_{us4}\right) \end{cases} \tag{15}$$

where z_{as0_i} $(i = 1, 2, 3, 4)$ is the initial air spring displacement, q_{in_i} and $q_{out\_i}(i = 1, 2, 3, 4)$ are the air mass flow into and out of the air spring of the i^{th}corner.

3) MODEL OF RANDOM ROAD EXCITATION FOR FOUR WHEELS

It is well-known that the heave and pitch motions of the vehicle caused by road roughness affect the comfort and the safety of passengers. Excitation of the vertical vibration is generated due to road surface roughness. Road excitation can be modeled as a mechanical system that characterized by the coefficient of the road surface roughness, speed of the vehicle, wheelbase and track width.

A road profile based on the input spectral density of four wheels and correlation function with the track between left and right wheels is developed under an approximation method [33], as follows,

$$\dot{z}_{r\_2}(t) = -\frac{v}{2b}z_{r\_2}(t) + e^{-4\pi n_{00}b}z_{r\_2}(t) \tag{16}$$

where v represents the velocity of the vehicle, b is the half-track width, and n_{00} is the cut-off frequency of road space.

Assuming the vehicle is driving under straight line condition, the road profile for rear wheels is roughly the same as front wheels, but a time delay is involved in this process. Therefore, the relationship of road profile between rear and front wheels at a constant speed v can be expressed as follows,

$$\begin{cases} z_{r\_3}(t) = z_{r\_1}(t-\tau) = z_{r\_1}\left(t - \frac{a_1+a_2}{v}\right) \\ z_{r\_4}(t) = z_{r\_2}(t-\tau) = z_{r\_2}\left(t - \frac{a_1+a_2}{v}\right) \end{cases} \tag{17}$$

where $\tau = \frac{a_1+a_2}{v}$ is the lag time.

The transfer function between the input and output based on the time delay system with Eq. (17) can be obtained by the second order Pade algorithm [34]

$$\begin{cases} G_{31}(s) = \dfrac{z_{r\_3}(s)}{z_{r\_1}(s)} = \dfrac{1 - \frac{\tau}{2}s + \frac{\tau^2}{12}s^2}{1 + \frac{\tau}{2}s + \frac{\tau^2}{12}s^2} \\ G_{42}(s) = \dfrac{z_{r\_4}(s)}{z_{r\_2}(s)} = \dfrac{1 - \frac{\tau}{2}s + \frac{\tau^2}{12}s^2}{1 + \frac{\tau}{2}s + \frac{\tau^2}{12}s^2} \end{cases} \tag{18}$$

To use the above equation in time-domain, the state-space equation of Eq. (18) can be written as,

$$\begin{bmatrix} \dot{x}_1 \\ \dot{x}_2 \end{bmatrix} = \begin{bmatrix} 01 \\ -\frac{12}{\tau^2} \quad -\frac{6}{\tau} \end{bmatrix} \begin{bmatrix} x_1 \\ x_2 \end{bmatrix} + \begin{bmatrix} -\frac{12}{\tau} \\ \frac{72}{\tau^2} \end{bmatrix} z_{r\_1}(t) \quad (19)$$

$$z_{r\_3}(t) = [01] \begin{bmatrix} x_1 \\ x_2 \end{bmatrix} + z_{r\_1}(t) \quad (20)$$

where x_1 and x_2 are the state variables. Differentiating $z_{r\_3}(t)$ with respect to time, it yields,

$$\dot{z}_{r\_3}(t) = [01] \begin{bmatrix} \dot{x}_1 \\ \dot{x}_2 \end{bmatrix} + \dot{z}_{r\_1}(t) \quad (21)$$

Then, substituting Eq. (19) into Eq. (21)gives,

$$\dot{z}_{r\_3}(t) = [01] \begin{bmatrix} x_1 \\ x_2 \end{bmatrix} - \frac{12}{\tau} z_{r\_1}(t) + \dot{z}_{r\_1}(t) \quad (22)$$

Similarly, the relationship of road profile between right-rear wheel and right-front wheel can be expressed as,

$$\dot{z}_{r\_4}(t) = [01] \begin{bmatrix} x_1 \\ x_2 \end{bmatrix} - \frac{12}{\tau} z_{r\_2}(t) + \dot{z}_{r\_2}(t) \quad (23)$$

Therefore, the state-space equation with model of random road excitation for four wheels is determined by the aforementioned equations,

$$\begin{cases} \dot{z}_{r\_1}(t) = -0.111 v z_{r\_1}(t) - 4.44\sqrt{G_q(n_0)\, v}\, w(t) \\ \dot{z}_{r\_2}(t) = -\frac{v}{2b} z_{r\_2}(t) + e^{-4\pi n_{00} b} \frac{v}{2b} z_{r\_1}(t) \\ \dot{z}_{r\_3}(t) = x_2 - \frac{12}{\tau} z_{r\_1}(t) - 0.111 v z_{r\_1}(t) \\ \qquad -4.44\sqrt{G_q(n_0)\, v}\, w(t) \\ \dot{z}_{r\_4}(t) = x_2 - \frac{12}{\tau} z_{r\_2}(t) - \frac{v}{2b} z_{r\_2}(t) \\ \qquad + e^{-4\pi n_{00} b} \frac{v}{2b} z_{r\_1}(t) \\ \dot{x}_1 = x_2 - \frac{12}{\tau} z_{r\_1}(t) \\ \dot{x}_2 = -\frac{12}{\tau^2} x_1 - \frac{6}{\tau} x_2 + \frac{72}{\tau^2} z_{r\_1}(t) \\ x_r = \left[z_{r\_1} z_{r\_2} z_{r\_3} z_{r\_4} x_1(t)\, x_2(t) \right] \\ u_r = [w(t)] \\ y_r = \left[z_{r\_1} z_{r\_2} z_{r\_3} z_{r\_4} \right] \end{cases} \quad (24)$$

where x_r represents the state variable vector, u_r is the input variable vector and y_r is the output variable vector. $G_q(n_0)$ is the coefficient of road roughness, n_0 is the reference frequency, n_{00} is the cut-off frequency of road space. Hence, the state-space representation of the model with random road excitation for four wheels can be formulated as,

$$\begin{cases} \dot{x}_r = A_r x_r + B_r u_r \\ y_r = C_r x_r + D_r u_r \end{cases} \quad (25)$$

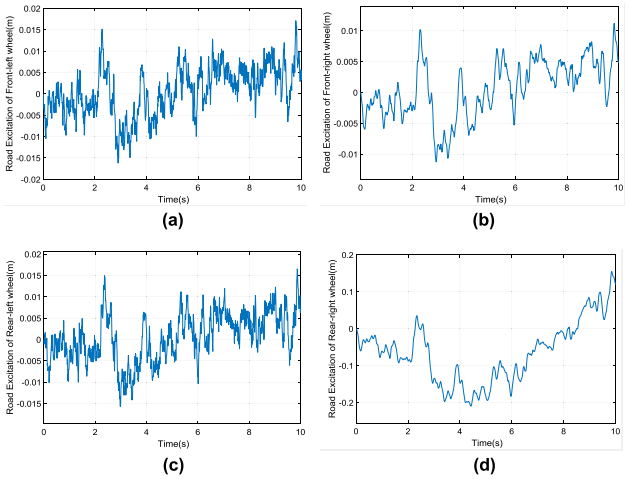

FIGURE 4. Random input of C-class road for four wheels. (a) Random input of front-left wheel. (b) Random input of front-right wheel. (c) Random input of rear-left wheel. (d) Random input of rear-right wheel.

TABLE 1. Simulation parameters for road excitation of four wheels.

Parameter	Value	Unit	Parameter	Value	Unit
v	14	m/s	n_{00}	0.01	m^{-1}
a_1	1.062	m	a_2	1.638	m
b	0.7775	m	τ	0.09	s
$G_q(n_0)$	0.000256	m^3	π	3.14	–

The detailed description of A_r, B_r, C_r and D_r are given as follows,

$$A_r = \begin{bmatrix} -\frac{v}{2b} & e^{-4\pi n_{00} b} \frac{v}{2b} & 0 & 0 & 0 & 0 \\ 0 & -0.111v & 0 & 0 & 0 & 0 \\ 0 & -\frac{12}{\tau} - 0.111v & 0 & 0 & 0 & 1 \\ -\frac{12}{\tau} - \frac{v}{2b} & e^{-4\pi n_{00} b} \frac{v}{2b} & 0 & 0 & 0 & 1 \\ 0 & -\frac{12}{\tau} & 0 & 0 & 0 & 1 \\ 0 & -\frac{72}{\tau^2} & 0 & 0 & -\frac{12}{\tau^2} & -\frac{6}{\tau} \end{bmatrix}$$

$$B_r = \begin{bmatrix} 0 \\ -4.44\sqrt{G_q(n_0)\, v} \\ -4.44\sqrt{G_q(n_0)\, v} \\ 0 \\ 0 \\ 0 \end{bmatrix}$$

$$C_r = \begin{bmatrix} 1 & 0 & 0 & 0 & 0 & 0 \\ 0 & 1 & 0 & 0 & 0 & 0 \\ 0 & 0 & 1 & 0 & 0 & 0 \\ 0 & 0 & 0 & 1 & 0 & 0 \end{bmatrix} \quad D_r = \begin{bmatrix} 0 \\ 0 \\ 0 \\ 0 \end{bmatrix} \quad (26)$$

Figure 4. shows the simulation results of the random input of C-class road for the four wheels. The simulation parameters of the vehicle and C-class road are shown in Table 1.

The C-class road is one of the typical road profiles to test the vertical performance of vehicles and the parameters in Table 1 are used to generate a standard C-class road profile.

C. LINEARIZATION FOR THE MODEL OF RIDE HEIGHT ADJUSTMENT SYSTEM

In order to design a NMPC on the basis of the linear state-space equation and determine an optimal solution by using quadratic programming, the nonlinear parts in the vehicle model should be linearized firstly.

For small roll and pitch angles, the following linear geometrical relationships are expressed as,

$$\begin{cases} z_{s1} = z_s + a_1\theta + b\phi \\ z_{s2} = z_s + a_1\theta - b\phi \\ z_{s3} = z_s - a_2\theta + b\phi \\ z_{s4} = z_s - a_2\theta - b\phi \end{cases} \tag{27}$$

Therefore, the dynamic equation of the full car model can be presented mathematically as,

$$\begin{cases} M_s\ddot{z}_s = p_{as1}A_{as1} + p_{as2}A_{as2} + p_{as3}A_{as3} + p_{as4}A_{as4} \\ \quad + C_{d1}\dot{z}_{us1} + C_{d2}\dot{z}_{us2} + C_{d3}\dot{z}_{us3} + C_{d4}\dot{z}_{us4} \\ \quad - (C_{d1} + C_{d2} + C_{d3} + C_{d4})\,\dot{z}_s \\ \quad - (C_{d1}a_1 + C_{d2}a_1 - C_{d3}a_2 - C_{d4}a_2)\,\dot{\theta} \\ \quad - (C_{d1} - C_{d2} + C_{d3} - C_{d4})\,b\dot{\phi} \\ I_y\ddot{\phi} = bp_{as1}A_{as1} - bp_{as2}A_{as2} + bp_{as3}A_{as3} - bp_{as4}A_{as4} \\ \quad + C_{d1}b\dot{z}_{us1} - C_{d2}b\dot{z}_{us2} + C_{d3}b\dot{z}_{us3} \\ \quad - C_{d4}b\dot{z}_{us4} - (C_{d1} - C_{d2} + C_{d3} - C_{d4})\,b\dot{z}_s \\ \quad - (C_{d1}a_1 - C_{d2}a_1 - C_{d3}a_2 + C_{d4}a_2)\,b\dot{\theta} \\ \quad - (C_{d1} + C_{d2} + C_{d3} + C_{d4})\,b^2\dot{\phi} \\ I_y\ddot{\theta} = a_1p_{as1}A_{as1} + a_1p_{as2}A_{as2} - a_2p_{as3}A_{as3} - a_2p_{as4}A_{as4} \\ \quad + C_{d1}a_1\dot{z}_{us1} + C_{d2}a_1\dot{z}_{us2} - C_{d3}a_2\dot{z}_{us3} - C_{d4}a_2\dot{z}_{us4} \\ \quad - (C_{d1}a_1 + C_{d2}a_1 - C_{d3}a_2 - C_{d4}a_2)\,\dot{z}_s \\ \quad - \left(C_{d1}a_1^2 + C_{d2}a_1^2 + C_{d3}a_2^2 + C_{d4}a_2^2\right)\dot{\theta} \\ \quad - (C_{d1}a_1 - C_{d2}a_1 - C_{d3}a_2 + C_{d4}a_2)\,b\dot{\phi} \\ m_{us1}\ddot{z}_{us1} = k\left(z_{r\_1} - z_{us1}\right) - p_{as1}A_{as1} - C_{d1}\dot{z}_{us1} + C_{d1}\dot{z}_s \\ \quad + C_{d1}a_1\dot{\theta} + C_{d1}b\dot{\phi} \\ m_{us2}\ddot{z}_{us2} = k\left(z_{r\_2} - z_{us2}\right) - p_{as2}A_{as2} - C_{d2}\dot{z}_{us2} + C_{d2}\dot{z}_s \\ \quad + C_{d2}a_1\dot{\theta} - C_{d2}b\dot{\phi} \\ m_{us3}\ddot{z}_{us3} = k\left(z_{r\_3} - z_{us3}\right) - p_{as3}A_{as3} - C_{d3}\dot{z}_{us3} + C_{d3}\dot{z}_s \\ \quad - C_{d3}a_1\dot{\theta} + C_{d3}b\dot{\phi} \\ m_{us4}\ddot{z}_{us4} = k\left(z_{r\_4} - z_{us4}\right) - p_{as4}A_{as4} - C_{d4}\dot{z}_{us4} + C_{d4}\dot{z}_s \\ \quad - C_{d4}a_1\dot{\theta} - C_{d4}b\dot{\phi} \end{cases} \tag{28}$$

During the gas charging and discharging processes, both the air pressure in air spring and the air spring volume are variables, and the nonlinear dynamic behavior of the air spring can be reflected as Eq. (13). In order to linearize the model of the air spring, the dynamic characteristics of some variables in Eq. (13) have to be ignored. Since the rate of change of the air pressure $\dot{p}_{as}$ and the rate of change of the air spring displacement $\dot{z}_{as}$ have a significant influence on the whole system, these time-varying variables should be kept. Therefore, the other two variables, p_{as} and z_{as}, should be considered in this system as well. By substituting p_{as0}, which refers to the initial air pressure in the air spring, for p_{as}, and substituting zero for z_{as}, a linear equation for the air spring model can be obtained as follows,

$$\dot{p}_{as}A_{as}z_{as0} = \kappa RT\left(q_{in} - q_{out}\right) - \kappa p_{as0}A_{as}\left(\dot{z}_s - \dot{z}_{us}\right) \tag{29}$$

The premise of replacing Eq. (13) with the linear form of Eq. (28) is that it has a minor error on the dynamic evolution of the ride height and posture adjustment system, but it can ease the optimization process in NMPC. In order to verify this, two different models of the quarter vehicle model are built in Matlab/Simulink based on Eq. (13) and Eq. (28), respectively.

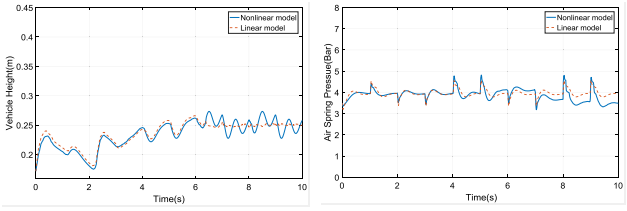

(a) (b)

FIGURE 5. Simulation results comparison between two models. (a) Vehicle height. (b) Air pressure in air spring.

TABLE 2. Simulation parameters for quarter vehicle model.

Parameter	Value	Unit	Parameter	Value	Unit
m_s	300	kg	κ	1.4	-
R	287.05	$J/kg\cdot K$	T	293.15	k
C	2450	$N\cdot s/m$	m_u	30	kg
A_{as}	0.0072	m^2	P_{as0}	350000	pa
k	26800	$k\cdot N/m$	P_t	800000	pa
P_{amt}	101330	pa			

Figure 5 shows the simulation results comparison between the two models, including the vehicle height of quarter vehicle and the air pressure in the air spring. The simulation parameters of the quarter vehicle model are shown in Table 2. It can be seen that the simulation result of the linear approximation model is in good agreement with the result of the nonlinear model, except for some points in the transient responses. In the vehicle ride height control problem, the steady-state response is more important than the transient

response, the small error in the transient performance is acceptable in the design of the controller in this study. Thus, the linear model can be used to predict the system dynamic behavior.

Hence, the linear model of the air spring for the full car can be expressed as,

$$\begin{cases} \dot{p}_{as1}A_{as1}z_{as0\_1} = \kappa RT\left(q_{in\_1} - q_{out\_1}\right) \\ \qquad\qquad -\kappa p_{as0\_1}A_{as1}\left(\dot{z}_{s1} - \dot{z}_{us1}\right) \\ \dot{p}_{as2}A_{as2}z_{as0\_2} = \kappa RT\left(q_{in\_2} - q_{out\_2}\right) \\ \qquad\qquad -\kappa p_{as0\_2}A_{as2}\left(\dot{z}_{s2} - \dot{z}_{us2}\right) \\ \dot{p}_{as3}A_{as3}z_{as0\_3} = \kappa RT\left(q_{in\_3} - q_{out\_3}\right) \\ \qquad\qquad -\kappa p_{as0\_3}A_{as3}\left(\dot{z}_{s3} - \dot{z}_{us3}\right) \\ \dot{p}_{as4}A_{as4}z_{as0\_4} = \kappa RT\left(q_{in\_4} - q_{out\_4}\right) \\ \qquad\qquad -\kappa p_{as0\_4}A_{as4}\left(\dot{z}_{s4} - \dot{z}_{us4}\right) \end{cases} \tag{30}$$

where $p_{as0\_i}\ (i = 1, 2, 3, 4)$ is the initial air pressure of air spring, and the rate of change of the sprung mass displacement $\dot{z}_{si}\ (i = 1, 2, 3, 4)$ can be obtained from Eq. (26), as follows,

$$\begin{cases} \dot{z}_{s1} = \dot{z}_s + a_1\dot{\theta} + b\dot{\phi} \\ \dot{z}_{s2} = \dot{z}_s + a_1\dot{\theta} - b\dot{\phi} \\ \dot{z}_{s3} = \dot{z}_s - a_2\dot{\theta} + b\dot{\phi} \\ \dot{z}_{s4} = \dot{z}_s - a_2\dot{\theta} - b\dot{\phi} \end{cases} \tag{31}$$

Finally, the linear model of the air spring for the full car can be described as,

$$\begin{cases} \dot{p}_{as1} = \dfrac{\kappa RT\left(q_{in\_1} - q_{out\_1}\right)}{A_{as1}z_{as0\_1}} - \dfrac{\kappa p_{as1}\dot{z}_s}{z_{as0\_1}} - \dfrac{\kappa a_1\dot{\theta}p_{as0\_1}}{z_{as0\_1}} \\ \qquad - \dfrac{\kappa b\dot{\phi}p_{as0\_1}}{z_{as0\_1}} + \dfrac{\kappa p_{as0\_1}\dot{z}_{us1}}{z_{as0\_1}} \\ \dot{p}_{as2} = \dfrac{\kappa RT\left(q_{in\_2} - q_{out\_2}\right)}{A_{as2}z_{as0\_2}} - \dfrac{\kappa p_{as2}\dot{z}_s}{z_{as0\_2}} - \dfrac{\kappa a_1\dot{\theta}p_{as0\_2}}{z_{as0\_2}} \\ \qquad + \dfrac{\kappa b\dot{\phi}p_{as0\_2}}{z_{as0\_2}} + \dfrac{\kappa p_{as0\_2}\dot{z}_{us2}}{z_{as0\_2}} \\ \dot{p}_{as3} = \dfrac{\kappa RT\left(q_{in\_3} - q_{out\_3}\right)}{A_{as3}z_{as0\_3}} - \dfrac{\kappa p_{as3}\dot{z}_s}{z_{as0\_3}} + \dfrac{\kappa a_2\dot{\theta}p_{as0\_3}}{z_{as0\_3}} \\ \qquad - \dfrac{\kappa b\dot{\phi}p_{as0\_3}}{z_{as0\_3}} + \dfrac{\kappa p_{as0\_3}\dot{z}_{us3}}{z_{as0\_3}} \\ \dot{p}_{as4} = \dfrac{\kappa RT\left(q_{in\_4} - q_{out\_4}\right)}{A_{as4}z_{as0\_4}} - \dfrac{\kappa p_{as4}\dot{z}_s}{z_{as0\_4}} + \dfrac{\kappa a_2\dot{\theta}p_{as0\_4}}{z_{as0\_4}} \\ \qquad + \dfrac{\kappa b\dot{\phi}p_{as0\_4}}{z_{as0\_4}} + \dfrac{\kappa p_{as0\_4}\dot{z}_{us4}}{z_{as0\_4}} \end{cases} \tag{32}$$

The state-space equation of the linear model for the RHC and posture adjustment system with the full car is determined by Eq. (27) and Eq. (13),

$$\begin{cases} \dot{x} = Ax + Bu + B_d d \\ y = Cx + Du \end{cases} \tag{33}$$

According to the linear equation expressed as Eq. (27), the linear model of the air spring obtained as Eq. (31) and the state-space equation presented as Eq.(33), the state variable vector is defined as follows,

$$x = [p_{as1}\ p_{as2}\ p_{as3}\ p_{as4}\ z_{us1}\ z_{us2}\ z_{us3}\ z_{us4}\ \dot{z}_{us1}\ \dot{z}_{us2}\ \dot{z}_{us3}\ \dot{z}_{us4}\ z_s\ \phi\ \theta\ \dot{z}_s\ \dot{\phi}\ \dot{\theta}]^T \tag{34}$$

The input variables are defined as follows,

$$u = \left[q_{in\_1} - q_{out\_1}q_{in\_2} - q_{out\_2}q_{in\_3} - q_{out\_3}q_{in\_4} - q_{out\_4}\right]^T \tag{35}$$

The output variables are defined based on the concerned system performance indices as,

$$\begin{aligned} y &= [z_{s1}z_{s2}z_{s3}z_{s4}z_s\phi\theta]^T \\ &= [z_s + a_1\theta + b\phi z_s + a_1\theta - b\phi z_s - a_2\theta \\ &\quad + b\phi z_s - a_2\theta - b\phi z_s\phi\theta] \end{aligned} \tag{36}$$

The disturbance of the system is expressed as,

$$d = \left[z_{r\_1}\ z_{r\_2}\ z_{r\_3}\ z_{r\_4}\right]^T \tag{37}$$

The detailed description of A, B, B_d, C and D are given in Appendix I.

III. CONTROLLER DESIGN

A. CONTROL OBJECTIVES

Aiming to improve ride comfort, fuel economy and handling safety of the vehicle, the bounce of vehicle body z_s, and the roll angle ϕ and pitch angle θ should be rapidly regulated to their reference with minimum error. Therefore, on the basis of the ride height and posture control law, the target of the SAAS system can be considered as:

$$\text{Objectives} \begin{cases} z_s\left(k\right) \to z_{ref}, \\ \phi\left(k\right) \to 0, \quad ask \to \infty \\ \theta\left(k\right) \to 0, \end{cases} \tag{38}$$

where k represents the current time.

In order to implement the desired SAAS system with acceptable fuel economy and ride comfort, some dynamic characteristics of the system should be considered. At this point, it is possible to apply the following constraints to the variables of the full car,

$$\begin{cases} z_{\min} \le z_s \le z_{\max} \\ z_{\min} \le z_{as\_i} \le z_{\max} \\ \phi_{\min} \le \phi \le \phi_{\max} \\ \theta_{\min} \le \theta \le \theta_{\max} \\ u_{\min} \le u\left(k\right) \le u_{\max} \end{cases} \tag{39}$$

where $z_{\min}, z_{\max}, \phi_{\min}, \phi_{\max}, \theta_{\min}, \theta_{\max}$ are the bounds of the bounce of vehicle body, roll and pitch angles. The minimum and maximum values of z_s, ϕ and θ are defined with the respect to the dynamic characteristic of the vehicle. $u\left(k\right)$ is the control input that should be bounded according to the air mass flow. The simulation parameters concerned are shown in Table. 3.

TABLE 3. Parameters of the NMPC.

Parameter	Value	Unit	Parameter	Value	Unit
$z_{\max}$	22	mm	$z_{\min}$	-32	mm
$\phi_{\max}$	0.02	deg	$\phi_{\min}$	-0.02	deg
$\theta_{\max}$	0.03	deg	$\theta_{\min}$	-0.03	deg
$u_{\max}$	0.015	kg/s	$u_{\min}$	-0.01	kg/s

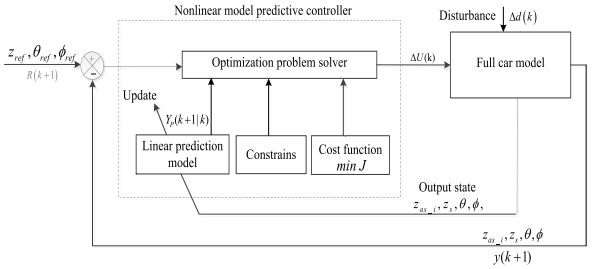

FIGURE 6. Schematic diagram of the proposed NMPC.

B. NMPC FOR SAAS SYSTEMS

The control scheme is summarized in Figure 6. In the proposed NMPC scheme, a linear model of the full car is used to predict the future state of the system. Based on this prediction, the receding horizon policy can be achieved by using the current state of the car as the initial state and re-computing the control sequence at the next sampling instant [23]. Given the ride height position z_{ref}, desired roll angle θ_{ref} and desired pitch angles ϕ_{ref}, the control objective is to manipulate the ride height z_s, roll θ and pitch angles ϕ to their reference as fast and stable as possible. There are three parts of the nonlinear model predictive controller including predictive model, constraints and cost function. During the transitional state, the reference $R_f\,(k+1)$ is described as the control objective, the disturbance $\Delta d\,(k)$ is the random road excitation. The output is $y\,(k+1)$, which are the relative sprung mass displacement, the roll and pitch angles. A nonlinear model predictive controller is to design to determine the control commands $\Delta U\,(k)$ as the control input vector to meet the requirement of the aforesaid objective. Then, the time horizon moves one step ahead and repeats.

The function of the proposed SAAS system is to compute the dynamic control commands and subsequently manipulates the relative ride height, the roll and pitch angles. This function can be formulated as an optimization problem.

The basic principle of NMPC is that the current control action is obtained by solving an optimization problem, and the value of the solved incremental control signal $\Delta U\,(k)$ is firstly applied. The further system state $Y_P(k+1|k)$ are predicted based on the aforesaid linear model and the current state $x\,(k)$. Therefore, the incremental equation of the linear prediction model is represented as,

$$\begin{cases} \Delta x\,(k+1) = A\Delta x\,(k) + B_u\Delta u\,(k) + B_c\Delta d\,(k) \\ y\,(k) = C_c\Delta x\,(k) + y\,(k-1) \end{cases} \tag{40}$$

where the change of system state is $\Delta x\,(k) = x\,(k) - x\,(k-1)$, the change of control input is $\Delta u\,(k) = u\,(k) - u\,(k-1)$, and the change of system disturbance is $\Delta d\,(k) = d\,(k) - d\,(k-1)$. Moreover, A_x, B_u, B_c and C_c are system matrices, which can be expressed as,

$$\begin{aligned} A_x &= e^{AT_s}, \\ B_u &= \int_0^{T_s} e^{A\tau}d\tau \cdot B, \\ B_c &= \int_0^{T_s} e^{A\tau}d\tau \cdot B_d, \\ C_c &= C \end{aligned} \tag{41}$$

where T_s is sampling time.

In addition, the predicted performance vector $Y_P(k+1|k)$ and the change of control input $\Delta U\,(k)$ of the SAAS system at k, which k represents the k_{th} sampling time, are calculated as,

$$\begin{cases} Y_P\,(k+1|k) = \begin{bmatrix} y_p\,(k+1|k) \\ y_p\,(k+2|k) \\ \vdots \\ y_p\,(k+p|k) \end{bmatrix}_{p\times 1} \\ \Delta U\,(k) = \begin{bmatrix} \Delta u\,(k) \\ \Delta u\,(k+1) \\ \vdots \\ \Delta u\,(k+m-1) \end{bmatrix}_{m\times 1} \end{cases} \tag{42}$$

where p is the predicted horizon, m is the control horizon, the predictive performance at the time k are $y_p\,(k+1|k), y_p\,(k+2|k), \cdots, y_p\,(k+p|k)$, the change of command sequence of the control signal are $\Delta u\,(k)$, $\Delta u\,(k+1), \cdots, \Delta u\,(k+m-1)$. Moreover, the predictive output performance vector is,

$$Y_p\,(k+1|k) = \mathbf{S_x}\Delta x\,(k) + \mathbf{I}y\,(k) + \mathbf{S_d}\Delta d\,(k) + \mathbf{S_u}\Delta U\,(k) \tag{43}$$

where $\mathbf{S_x}$, $\mathbf{I}$, $\mathbf{S_d}$ and $\mathbf{S_u}$ are the matrix parameters, which are described in Appendix II.

At the sampling time k, the current disturbance, which is the random road excitation $\Delta d\,(k)$, is not measured at the sampling time $k-1$. The relationship between the current disturbance and its previous state can be expressed as,

$$d\,(k) = d\,(k-1|k) \tag{44}$$

In order to obtain the optimal control input based on the performance of the prediction model, the following performance index is required to be minimized in the NMPC.

$$\begin{aligned} J\,(x\,(k), \Delta U\,(k)) = &\left\|\Gamma_y\,(Y_P\,(k+1|k) - R\,(k+1))\right\|^2 \\ &+ \left\|\Gamma_u\Delta U\,(k)\right\|^2 \end{aligned} \tag{45}$$

where $R\,(k+1)$ is the reference vector relative to each output vector at sampling time $k+1$, Γ_y and Γ_u are the weight matrix of output and input incremental, respectively.

TABLE 4. Simulation parameters of full car.

Parameter	Value	Unit	Parameter	Value	Unit
M_s	1314	kg	κ	1.4	—
R	287.05	$J/kg \cdot K$	T	293.15	K
C_{d1},C_{d2}	2450	$N \cdot s/m$	C_{d3},C_{d4}	1893	$N \cdot s/m$
b	0.7775	m	a_1	1.062	m
a_2	1.638	m	I_v	493	$kg \cdot m^2$
I_y	2122	$kg \cdot m^2$	A_{as1}, A_{as2}	0.0072	m^2
A_{as3}, A_{as4}	0.0079	m^2	m_{us1}, m_{us2}	30	kg
m_{us4}, m_{us4}	20	kg	z_{as0_1}, z_{as0_2}	0.1716	m
z_{as0_3}, z_{as0_4}	0.1305	m	p_{as0_1}, p_{as0_2}	350000	pa
p_{as0_3}, p_{as0_4}	180000	pa	k	26800	$k \cdot N/m$

The cost function can be obtained from Eq. (43) and Eq. (45), as follows,

$$\begin{aligned} &J\left(x\left(k\right),\Delta U\left(k\right)\right) \\ &\quad=\left\|\Gamma_y\left(\mathbf{S}_x\Delta x\left(k\right)+\mathbf{I}y\left(k\right)+\mathbf{S}_d\Delta d\left(k\right)\right.\right. \\ &\qquad\left.\left.+\mathbf{S}_u\Delta U\left(k\right)-R_f\left(k+1\right)\right)\right\|^2+\left\|\Gamma_u\Delta U\left(k\right)\right\|^2 \end{aligned} \tag{46}$$

Definine $E_P\left(k+1|k\right)=R_f\left(k+1\right)-\mathbf{S}_x\Delta x\left(k\right)-\mathbf{I}y\left(k\right)-\mathbf{S}_d\Delta d\left(k\right)$, the cost function can therefore be described as,

$$\begin{aligned} &\min J\left(x\left(k\right),\Delta U\left(k\right)\right) \\ &=\left\|\Gamma_y\left(\mathbf{S}_u\Delta U\left(k\right)-E_P\left(k+1|k\right)\right)\right\|^2+\left\|\Gamma_u\Delta U\left(k\right)\right\|^2 \\ &=\Delta U\left(k\right)^T\mathbf{S}_u^T\Gamma_y^T\Gamma_y\mathbf{S}_u\Delta U\left(k\right)+\Delta U\left(k\right)^T\Gamma_y^T\Gamma_y\Delta U\left(k\right) \\ &\quad-2E_P\left(k+1|k\right)^T\Gamma_y^T\Gamma_y\mathbf{S}_u\Delta U\left(k\right) \\ &\quad+E_P\left(k+1|k\right)^T\Gamma_y^T\Gamma_yE_P\left(k+1|k\right) \end{aligned} \tag{47}$$

The ideal goal of Eq. (47) is to simultaneously improve the ride comfort and fuel economy during the transitional maneuver. The optimal control signal can be calculated via the quadratic programming. Moreover, the last term in Eq. (51), $E_P\left(k+1|k\right)^T\Gamma_y^T\Gamma_yE_P\left(k+1|k\right)$, is independent of $\Delta U\left(k\right)$ and does not affect the calculation of $\Delta U\left(k\right)$ in the quadratic programming. Therefore, the cost function in Eq. (51) is simplified as follows,

$$\begin{aligned} &\min_{\Delta U(k)}\left(\Delta U\left(k\right)^T H\Delta U\left(k\right)-G\left(k+1|k\right)^T\Delta U\left(k\right)\right) \\ &Subject\ to\ C_u\Delta U\left(k\right)\geq b\left(k+1|k\right) \end{aligned} \tag{48}$$

where $H=\mathbf{S}_u^T\Gamma_y^T\Gamma_y\mathbf{S}_u+\Gamma_u^T\Gamma_u$, $G\left(k+1|k\right)=2\mathbf{S}_u^T\Gamma_y^T\Gamma_yE_p\left(k+1|k\right)$. Actually, Γ_y and Γ_u are the weight of control output and input, and they are usually tuned by the designer, so that different users can obtain various optimal results. C_u and $b\left(k+1|k\right)$ are the parameters of constraints described in Appendix III.

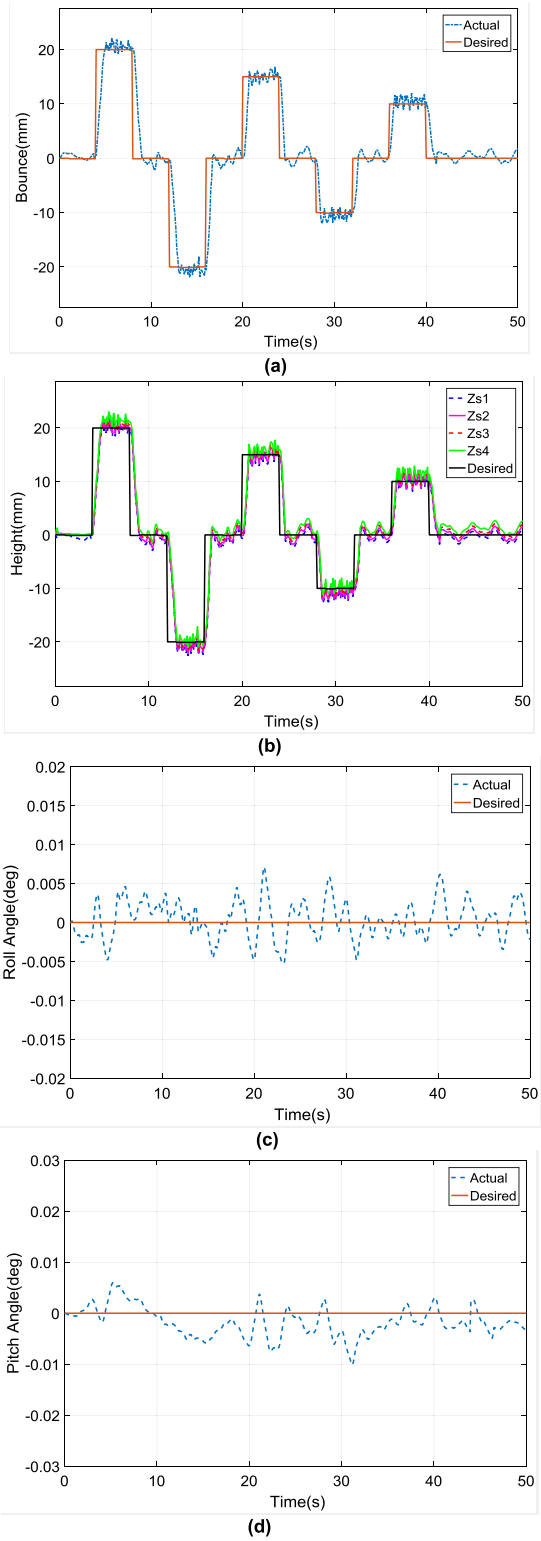

FIGURE 7. Simulation result of NMPC with C-class road input. (a) Vehicle bounce. (b) Displacement of four wheels. (c) Vehicle roll angle. (d) Vehicle pitch angle.

C. STABLILITY ANALYSIS

As mentioned in [35], due to computational reasons, the optimal control problem of NMPC has a finite horizon. Hence, the stability for the resultant controller is tough to prove. However, the stability is achieved in many applications since the constraints of the controller usually exist and

TABLE 5. Ziegler-Nichols method.

Control Type	K_P	T_i	T_d
P	$0.5K_u$	-	-
PI	$0.45K_u$	$T_u/1.2$	-
PD	$0.8K_u$ K_u	-	$T_u/8$
Classic PID	$0.6K_u$	$T_u/2$	$T_u/8$
Integral Rule	$0.7K_u$	$T_u/2.5$	$3T_u/20$
Some overshoot	$0.33K_u$	$T_u/2$	$T_u/3$
No overshoot	$0.2K_u$	$T_u/2$	$T_u/3$

TABLE 6. Comparison between PID and NMPC for bounce, roll and pitch angle.

Controller	Parameter	Unit	Desired value	MSAE	Maximum % of overshoot
NMPC	Bounce	mm	0	0.2157	-
PID				0.5987	-
NMPC	Bounce	mm	20	0.2382	1.19%
PID				0.6104	3.05%
NMPC	Bounce	mm	-20	0.2235	1.12%
PID				0.6438	3.22%
NMPC	Bounce	mm	15	0.1549	1.03%
PID				0.7033	4.69%
NMPC	Bounce	mm	-10	0.1382	1.38%
PID				0.6221	6.22%
NMPC	Bounce	mm	10	0.1186	1.19%
PID				0.6021	6.02%
NMPC	Roll angle	deg	0	0.000162	-
PID				0.000283	-
NMPC	Pitch angle	deg	0	0.000371	-
PID				0.000749	-

the horizons optimization is normally very long. Generally, two kinds of methods are applied to ensure the stability of NMPC. That is to achieve nominal stability for NMPC with additional terminal constraints, or to extend the optimization horizons [36].

Typically, most researches choose the first method to prove the system stability of NMPC. Just like the description in [37], a nonlinear model predictive controller was applied to guide a fixed-wing unmanned aerial vehicles in precision deep stall landing. It guarantees the stability of the control system by providing a hard constraint which limits the output to a specific bounded range. Besides, a model predictive control approach was applied to aircraft motion control [38]. In this paper, a novel model predictive,control scheme for aircraft motion control was developed. The control method satisfies the constraints which are related to aircraft physical limitations and passengers comfort so that the aircraft could be steered from some origin positions to a target destination. Although a strict mathematical proof for system stability has not been available yet, it is certain that the stability of the system is acknowledged since the constraints are imposed on aircraft motion.

TABLE 7. Comparison between PID and NMPC for displacement of four wheels.

Controller	Parameter	Unit	Desired value	MSAE	Maximum % of overshoot
NMPC	z_{s1}	mm	0	0.2153	-
PID				0.6297	-
NMPC	z_{s2}	mm	0	0.1965	-
PID				0.6039	-
NMPC	z_{s3}	mm	0	0.2025	-
PID				0.6149	-
NMPC	z_{s4}	mm	0	0.2284	-
PID				0.6215	-
NMPC	z_{s1}	mm	20	0.2312	1.16%
PID				0.6853	3.43%
NMPC	z_{s2}	mm	20	0.2471	1.24%
PID				0.7093	3.55%
NMPC	z_{s3}	mm	20	0.2262	1.13%
PID				0.6986	3.49%
NMPC	z_{s4}	mm	20	0.2185	1.09%
PID				0.7146	3.57%
NMPC	z_{s1}	mm	-20	0.2037	1.02%
PID				0.6983	3.49%
NMPC	z_{s2}	mm	-20	0.2146	1.07%
PID				0.7043	3.52%
NMPC	z_{s3}	mm	-20	0.1945	0.97%
PID				0.6992	3.50%
NMPC	z_{s4}	mm	-20	0.2203	1.10%
PID				0.7128	3.56%
NMPC	z_{s1}	mm	15	0.1739	1.16%
PID				0.6944	4.63%
NMPC	z_{s2}	mm	15	0.1687	1.12%
PID				0.7062	4.71%
NMPC	z_{s3}	mm	15	0.1594	1.06%
PID				0.7238	4.83%
NMPC	z_{s4}	mm	15	0.1486	0.99%
PID				0.7031	4.69%
NMPC	z_{s1}	mm	-10	0.1172	1.17%
PID				0.6835	6.84%
NMPC	z_{s2}	mm	-10	0.1204	1.20%
PID				0.7061	7.06%
NMPC	z_{s3}	mm	-10	0.1063	1.06%
PID				0.7182	7.18%
NMPC	z_{s4}	mm	-10	0.1114	1.11%
PID				0.6957	6.96%
NMPC	z_{s1}	mm	10	0.1096	1.10%
PID				0.7012	7.01%
NMPC	z_{s2}	mm	10	0.1027	1.02%
PID				0.6839	6.84%
NMPC	z_{s3}	mm	10	0.1044	1.04%
PID				0.7121	7.12%
NMPC	z_{s4}	mm	10	0.1079	1.08%
PID				0.7074	7.07%

In this research, the NMPC for the SAAS system takes into account the constraints which are physical limitations of the vehicle and comfort requirements. The details of the constraints are described in Eq. (43), and Table 3 state the constraints to variables and the parameters, respectively. Then, an optimization problem with the above mentioned constraints is developed. After computation, the target outputs of this control system are kept within limited ranges. It is believed that the system finally does not have any divergence and the system stability is implicitly guaranteed.

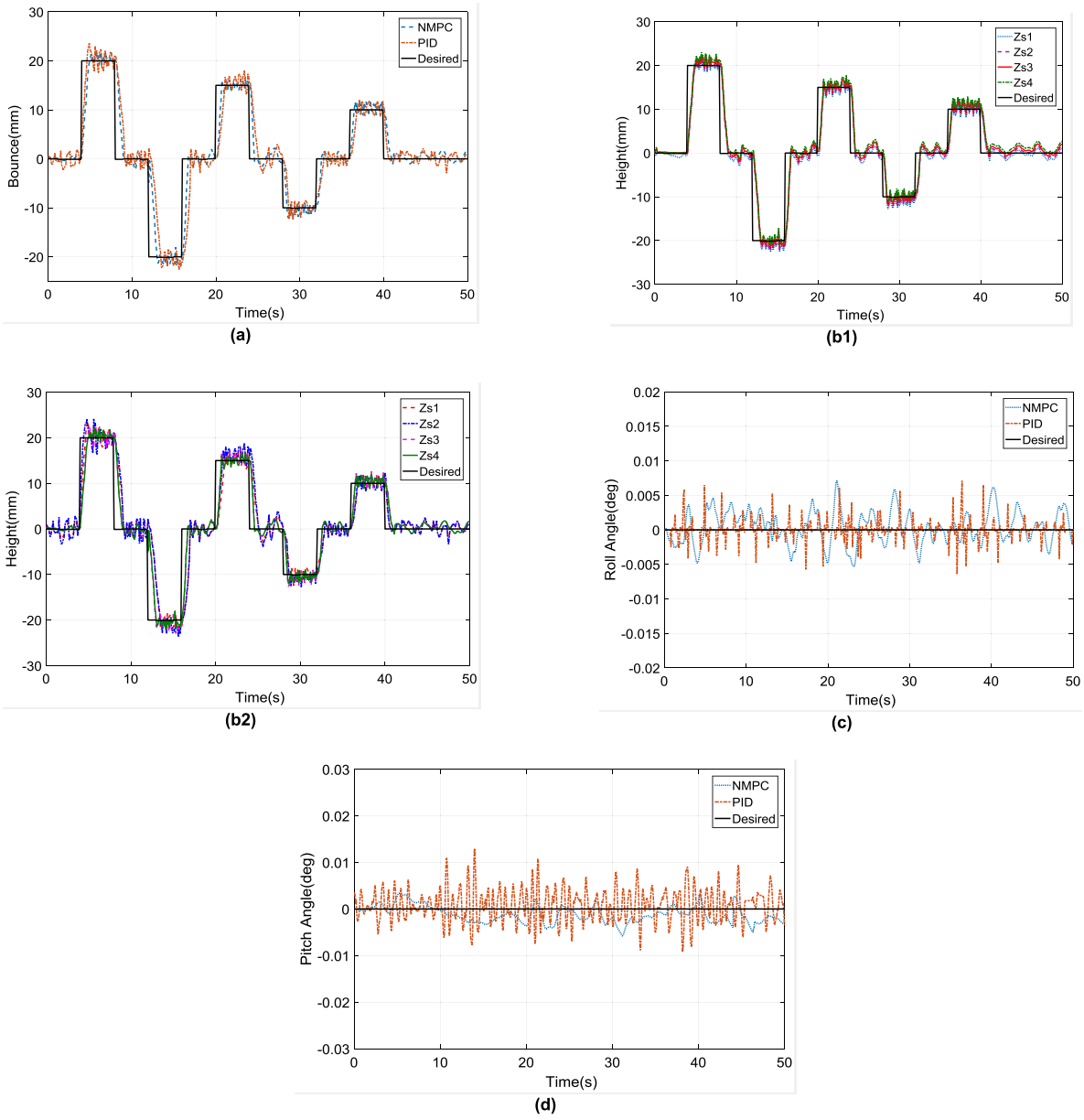

FIGURE 8. Simulation results of PID and NMPC. (a) Vehicle bounce. (b1) NMPC Control. (b2) PID control. (c) Vehicle roll angle. (d) Vehicle pitch angle.

IV. SIMULATIONS AND ANALYSIS

When the model of the SAAS system and its controller are successfully implemented, some simulation and experimental tests should be carried out to verify the effectiveness of the proposed NMPC. However, a test bench for a full car is time-consuming, high cost and bulky. To exactly examine the performance of the proposed control method without too much resource, simulation tests with Matlab/Simulink are conducted. In this Section, the relative ride height of the test car as well as the roll angle and pitch angle tests are condute with the established SAAS system. Then, the proposed controller is also compared with PID [18] method under the same simulation condition.

A. MATLAB/SIMULINK VERFIFICATION OF NMPC FOR SAAS SYSTEMS

1) SIMULATION SETUP

As shown in Figure 4, the random road excitation input of the SAAS system is given. The control objective is to track the desired height with minimum error and to regulate the roll and pitch angles of the vehicle body, despite the payload variation. Meanwhile, the simulation parameters of the ride height control and posture adjustment system and the target vehicle are given in Table 4.

2) SIMULATION RESULT OF SAAS SYSTEM WITH NMPC

In the aforesaid cost function, the weights Γ_y and Γ_u make difference performance for the system. Assuming that at the

$$A = \begin{bmatrix}
0 & 0 & 0 & 0 & 0 & 0 & 0 & 0 & \frac{kp_{as0_1}}{z_{as0_1}} & 0 & 0 & 0 & 0 & 0 & 0 & -\frac{kp_{as0_1}}{z_{as0_1}} & -\frac{kp_{as0_1}b}{z_{as0_1}} & -\frac{kp_{as0_1}a_1}{z_{as0_1}} \\
0 & 0 & 0 & 0 & 0 & 0 & 0 & 0 & 0 & \frac{kp_{as0_2}}{z_{as0_2}} & 0 & 0 & 0 & 0 & 0 & -\frac{kp_{as0_2}}{z_{as0_2}} & \frac{kp_{as0_2}b}{z_{as0_2}} & -\frac{kp_{as0_2}a_1}{z_{as0_2}} \\
0 & 0 & 0 & 0 & 0 & 0 & 0 & 0 & 0 & 0 & \frac{kp_{as0_3}}{z_{as0_3}} & 0 & 0 & 0 & 0 & -\frac{kp_{as0_3}}{z_{as0_3}} & -\frac{kp_{as0_3}b}{z_{as0_3}} & \frac{kp_{as0_3}a_2}{z_{as0_3}} \\
0 & 0 & 0 & 0 & 0 & 0 & 0 & 0 & 0 & 0 & 0 & \frac{kp_{as0_4}}{z_{as0_4}} & 0 & 0 & 0 & -\frac{kp_{as0_4}}{z_{as0_4}} & \frac{kp_{as0_4}b}{z_{as0_4}} & \frac{kp_{as0_4}a_2}{z_{as0_4}} \\
0 & 0 & 0 & 0 & 0 & 0 & 0 & 0 & 1 & 0 & 0 & 0 & 0 & 0 & 0 & 0 & 0 & 0 \\
0 & 0 & 0 & 0 & 0 & 0 & 0 & 0 & 0 & 1 & 0 & 0 & 0 & 0 & 0 & 0 & 0 & 0 \\
0 & 0 & 0 & 0 & 0 & 0 & 0 & 0 & 0 & 0 & 1 & 0 & 0 & 0 & 0 & 0 & 0 & 0 \\
0 & 0 & 0 & 0 & 0 & 0 & 0 & 0 & 0 & 0 & 0 & 1 & 0 & 0 & 0 & 0 & 0 & 0 \\
-\frac{A_{as1}}{m_{us1}} & 0 & 0 & 0 & -\frac{k}{m_{us1}} & 0 & 0 & 0 & -\frac{C_{d1}}{m_{us1}} & 0 & 0 & 0 & 0 & 0 & 0 & \frac{C_{d1}}{m_{us1}} & \frac{C_{d1}b}{m_{us1}} & \frac{C_{d1}a_1}{m_{us1}} \\
0 & -\frac{A_{as2}}{m_{us2}} & 0 & 0 & 0 & -\frac{k}{m_{us2}} & 0 & 0 & 0 & -\frac{C_{d2}}{m_{us2}} & 0 & 0 & 0 & 0 & 0 & \frac{C_{d2}}{m_{us2}} & -\frac{C_{d2}b}{m_{us2}} & \frac{C_{d2}a_1}{m_{us2}} \\
0 & 0 & -\frac{A_{as3}}{m_{us3}} & 0 & 0 & 0 & -\frac{k}{m_{us3}} & 0 & 0 & 0 & -\frac{C_{d3}}{m_{us3}} & 0 & 0 & 0 & 0 & \frac{C_{d3}}{m_{us3}} & \frac{C_{d3}b}{m_{us3}} & -\frac{C_{d3}a_2}{m_{us3}} \\
0 & 0 & 0 & -\frac{A_{as4}}{m_{us4}} & 0 & 0 & 0 & -\frac{k}{m_{us4}} & 0 & 0 & 0 & -\frac{C_{d4}}{m_{us4}} & 0 & 0 & 0 & \frac{C_{d4}}{m_{us4}} & \frac{C_{d4}b}{m_{us4}} & -\frac{C_{d4}a_2}{m_{us4}} \\
0 & 0 & 0 & 0 & 0 & 0 & 0 & 0 & 0 & 0 & 0 & 0 & 0 & 0 & 0 & 1 & 0 & 0 \\
0 & 0 & 0 & 0 & 0 & 0 & 0 & 0 & 0 & 0 & 0 & 0 & 0 & 0 & 0 & 0 & 1 & 0 \\
0 & 0 & 0 & 0 & 0 & 0 & 0 & 0 & 0 & 0 & 0 & 0 & 0 & 0 & 0 & 0 & 0 & 1 \\
\frac{A_{as1}}{M_s} & \frac{A_{as2}}{M_s} & \frac{A_{as3}}{M_s} & \frac{A_{as4}}{M_s} & 0 & 0 & 0 & 0 & \frac{C_{d1}}{M_s} & \frac{C_{d2}}{M_s} & \frac{C_{d3}}{M_s} & \frac{C_{d4}}{M_s} & 0 & 0 & 0 & A_{11} & A_{12} & A_{13} \\
\frac{A_{as1}b}{I_y} & -\frac{A_{as2}b}{I_y} & \frac{A_{as3}b}{I_y} & -\frac{A_{as4}b}{I_y} & 0 & 0 & 0 & 0 & \frac{C_{d1}b}{I_y} & -\frac{C_{d2}b}{I_y} & \frac{C_{d3}b}{I_y} & -\frac{C_{d4}b}{I_y} & 0 & 0 & 0 & A_{21} & A_{22} & A_{23} \\
\frac{A_{as1}a_1}{I_y} & \frac{A_{as2}a_1}{I_y} & -\frac{A_{as3}a_2}{I_y} & -\frac{A_{as4}a_2}{I_y} & 0 & 0 & 0 & 0 & \frac{C_{d1}a_1}{I_y} & \frac{C_{d2}a_1}{I_y} & -\frac{C_{d3}a_2}{I_y} & -\frac{C_{d4}a_2}{I_y} & 0 & 0 & 0 & A_{31} & A_{32} & A_{33}
\end{bmatrix}$$

$$A_{11} = -\frac{C_{d1}+C_{d2}+C_{d3}+C_{d4}}{M_s} \quad A_{12} = \frac{(-C_{d1}+C_{d2}-C_{d3}+C_{d4})\,b}{M_s} \quad A_{13} = \frac{-C_{d1}a_1-C_{d2}a_1+C_{d3}a_2+C_{d4}a_2}{M_s}$$

$$A_{21} = \frac{(-C_{d1}+C_{d2}-C_{d3}+C_{d4})\,b}{I_v} \quad A_{22} = -\frac{(C_{d1}+C_{d2}+C_{d3}+C_{d4})\,b^2}{I_v} \quad A_{23} = \frac{(-C_{d1}a_1+C_{d2}a_1+C_{d3}a_2-C_{d4}a_2)\,b}{I_v}$$

$$A_{31} = \frac{-C_{d1}a_1-C_{d2}a_1+C_{d3}a_2+C_{d4}a_2}{I_y} \quad A_{32} = \frac{(-C_{d1}a_1+C_{d2}a_1+C_{d3}a_2-C_{d4}a_2)\,b}{I_y} \quad A_{33} = \frac{-C_{d1}a_1^2-C_{d2}a_1^2+C_{d3}a_2^2+C_{d4}a_2^2}{I_y}$$

$$C = \begin{bmatrix}
0 & 0 & 0 & 0 & 0 & 0 & 0 & 0 & 0 & 0 & 0 & 0 & 1 & b & a_1 & 0 & 0 & 0 \\
0 & 0 & 0 & 0 & 0 & 0 & 0 & 0 & 0 & 0 & 0 & 0 & 1 & b & a_1 & 0 & 0 & 0 \\
0 & 0 & 0 & 0 & 0 & 0 & 0 & 0 & 0 & 0 & 0 & 0 & 1 & b & a_2 & 0 & 0 & 0 \\
0 & 0 & 0 & 0 & 0 & 0 & 0 & 0 & 0 & 0 & 0 & 0 & 1 & b & a_2 & 0 & 0 & 0 \\
0 & 0 & 0 & 0 & 0 & 0 & 0 & 0 & 0 & 0 & 0 & 0 & 1 & 0 & 0 & 0 & 0 & 0 \\
0 & 0 & 0 & 0 & 0 & 0 & 0 & 0 & 0 & 0 & 0 & 0 & 0 & 1 & 0 & 0 & 0 & 0 \\
0 & 0 & 0 & 0 & 0 & 0 & 0 & 0 & 0 & 0 & 0 & 0 & 0 & 0 & 1 & 0 & 0 & 0
\end{bmatrix}$$

$$D = zeros\,(7, 8)$$

sampling time k, Γ_y and Γ_u are described as,

$$\Gamma_y(k) = \begin{bmatrix} w_d(k) & 0 & 0 & 0 \\ 0 & w_b(k) & 0 & 0 \\ 0 & 0 & w_r(k) & 0 \\ 0 & 0 & 0 & w_p(k) \end{bmatrix},$$
$$\Gamma_u(k) = w_u(k) \tag{49}$$

where $w_d(k)$ is the corresponding weight of the air spring displacement of the four corners, $w_b(k)$ is the corresponding weight of bounce of the vehicle body, $w_r(k)$ is the corresponding weight of roll angle, $w_p(k)$ is the corresponding weight of pitch angle and $w_u(k)$ is the corresponding weight of air mass flow. The weights for the simulation test are given as,

$$\begin{cases} w_d(k) = 1 \\ w_b(k) = 10 \\ w_r(k) = 1 \\ w_p(k) = 1 \\ w_u(k) = 10 \end{cases} \tag{50}$$

Figure 7 shows the simulation result when the vehicle is driven on a rough road at 14m/s, and the road excitation is C-class. The road surface profiles for the four wheels are produced by the model of random road excitation presented in Figure 4. In Figure 7 (a) and Figure 7 (b), the desired height of full car and the four wheels, and actual height are shown. It can be seen from Figure 7 (a) that the bounce of the vehicle

can effectively track the desired value with road excitation input during the lifting and lowering process by the proposed controller. As shown in Figure 7 (b), all the displacement errors of four wheels are less than 2mm. This result verifies that the displacements of the four wheels are well-regulated to the desired value. Moreover, Figure 7 (c) and Figure 7 (d) shows that the roll and pitch angles also change little as the vehicle height changes although a high-frequency excitation is excited by the road profile.

B. COMPARISON WITH PID CONTROLLER

The PID controller is the existing controller for the SAAS system. As shown in Table 5, the PID gains in the test were tuned by Ziegler Nichols method, where K_p is the proportional gain; T_i is the integration time; T_d is the derivative time; K_u is the ultimate gain, and T_u is the oscillation period. Moreover, the PID gains are shown as,

$$\begin{cases} K_p = 170 \\ T_i = 20 \quad (Charging\ process) \\ T_d = 0 \end{cases} \tag{51}$$

$$\begin{cases} K_p = 1000 \\ T_i = 850 \quad (Discharging\ process) \\ T_d = 0 \end{cases} \tag{52}$$

The simulation result of this comparison is illustrated in Figure 8. To evaluate the control performance, the sum of mean absolute error (MSAE) and the maximum % of overshoot of these two simulation results are calculated at the same test period via Eq. (53) and Eq.(54), respectively. The results are shown in Table 4 and Table 5

$$MSAE = \frac{\sum_{i=0}^{n} |y_{des} - y_i|}{i} \tag{53}$$

where n represents the number of sample values. The value of n is 50 here due to the simulation time is 50s in this study, and one data is selected per second.

$$max\ \%\ of\ overshoot = max\left\{\frac{|y_{des} - y|}{|y_{des}|} \times 100\%\right\} \tag{54}$$

According to Table 6 and Table 7, the maximum % of overshoot does not exist in most instances due to the fact that the desired value is zero. However, significant differences could be found in the MSAE.

In Figure 8, it is obvious that the NMPC has a faster dynamic response and smaller error than the PID controller. Under the control of the NMPC, the vehicle bounce and displacement of four wheels have no trouble to track the target vehicle height. Moreover, the roll and pitch angles are also well-maintained in a numerical range ($|\theta| < 0.01°$, $|\phi| < 0.02°$) during the height control process, as shown in Figure 8 (c) and Figure 8(d). According to Table 6 and Table 7, the typical PID controller has a very high MSAE for a bounce, displacement of four wheels and roll and pitch angles. The most likely cause of this result is that the slow convergence speed of the PID controller. Besides, the trajectory as shown in Figure 8 indicates that the performance of PID controller is more unsteady and unsmooth. The main reason for this result is the PID gains are related to the overshoot, oscillation and the steady-state error of the control system.

Generally, the simulation results show that the proposed NMPC can adjust the vehicle height and regulate the vehicle posture, which performs better than the PID controller. It is clear that NMPC can effectively handle the issue of system nonlinearity and find the optimal solution. Furthermore, Figure 8 depicts that all of the outputs, including vehicle bounce, the displacement of four wheels, roll and pitch angles, are all not beyond the limitations and keep a nominal steady.

V. CONCLUSIONS

In this research, an analytical nonlinear model of a full car with SAAS, which considers the nonlinearities behavior of the air spring, is established completely. With this model, the relationship among the air pressure, relative ride height and roll and pitch angles can be set up. Moreover, a control algorithm based on NMPC is designed for the proposed linear model, and satisfactory test results are achieved, and the efficiency of the proposed controller is validated. Besides, the simulation results are compared with NMPC and typical PID. The gains of PID are tuned by Ziegler Nichols method. Simulation results demonstrate that the proposed NMPC is effective in the SAAS system control and can overcome the drawbacks of traditional PID controller.

APPENDIX I

$A, A_{11}, A_{21}, A_{31}, C, D$, as shown at the top of the previous page.

$$B = \begin{bmatrix} \frac{\kappa RT}{A_{as1}z_{as0\_1}} & 0 & 0 & 0 \\ 0 & \frac{\kappa RT}{A_{as2}z_{as0\_2}} & 0 & 0 \\ 0 & 0 & \frac{\kappa RT}{A_{as3}z_{as0\_3}} & 0 \\ 0 & 0 & 0 & \frac{\kappa RT}{A_{as4}z_{as0\_4}} \\ 0 & 0 & 0 & 0 \\ 0 & 0 & 0 & 0 \\ 0 & 0 & 0 & 0 \\ 0 & 0 & 0 & 0 \\ 0 & 0 & 0 & 0 \\ 0 & 0 & 0 & 0 \\ 0 & 0 & 0 & 0 \\ 0 & 0 & 0 & 0 \\ 0 & 0 & 0 & 0 \\ 0 & 0 & 0 & 0 \\ 0 & 0 & 0 & 0 \\ 0 & 0 & 0 & 0 \\ 0 & 0 & 0 & 0 \\ 0 & 0 & 0 & 0 \end{bmatrix},$$

$$B_d = \begin{bmatrix} 0 & 0 & 0 & 0 \\ 0 & 0 & 0 & 0 \\ 0 & 0 & 0 & 0 \\ 0 & 0 & 0 & 0 \\ 0 & 0 & 0 & 0 \\ 0 & 0 & 0 & 0 \\ 0 & 0 & 0 & 0 \\ 0 & 0 & 0 & 0 \\ \frac{k}{m_{us1}} & 0 & 0 & 0 \\ 0 & \frac{k}{m_{us2}} & 0 & 0 \\ 0 & 0 & \frac{k}{m_{us3}} & 0 \\ 0 & 0 & 0 & \frac{k}{m_{us4}} \\ 0 & 0 & 0 & 0 \\ 0 & 0 & 0 & 0 \\ 0 & 0 & 0 & 0 \\ 0 & 0 & 0 & 0 \\ 0 & 0 & 0 & 0 \\ 0 & 0 & 0 & 0 \end{bmatrix}$$

APPENDIX II

$$\mathbf{S_x} = \begin{bmatrix} CA \\ CA^2 + CA \\ \vdots \\ \vdots \\ \sum_{i=1}^{p} CA^{i-1} \end{bmatrix}_{p\times 1}, \quad \mathbf{I} = \begin{bmatrix} I_{n_c\times n_c} \\ I_{n_c\times n_c} \\ \vdots \\ I_{n_c\times n_c} \end{bmatrix}_{p\times 1},$$

$$\mathbf{S_d} = \begin{bmatrix} CB_d \\ CAB_d + CB_d \\ \vdots \\ \sum_{i=1}^{p} CA^{i-1}B_d \end{bmatrix}_{p\times 1}$$

$$\mathbf{S_u} = \begin{bmatrix} CB_u & 0 & \cdots & 0 \\ \sum_{i=1}^{2} CA^{i-1}B_u & CB_u & \cdots & 0 \\ \vdots & \vdots & \vdots & \vdots \\ \sum_{i=1}^{m} CA^{i-1}B_u & \sum_{i=1}^{m-1} CA^{i-1}B_u & \cdots & 0 \\ \vdots & \vdots & \vdots & \vdots \\ \sum_{i=1}^{p} CA^{i-1}B_u & \sum_{i=1}^{p-1} CA^{i-1}B_u & \cdots & \sum_{i=1}^{p-m+1} CA^{i-1}B_u \end{bmatrix}_{p\times m}$$

APPENDIX III

$$C_u = \left[-\mathbf{T}^T \ \mathbf{T}^T \ -\mathbf{L}^T \ \mathbf{L}^T \ -\mathbf{S_u^T} \ \mathbf{S_u^T}\right]^T_{(4m+2p)\times 1}$$

$$T = \begin{bmatrix} I_{n_u\times n_u} & \mathbf{0} & \cdots & \mathbf{0} \\ \mathbf{0} & I_{n_u\times n_u} & \cdots & \mathbf{0} \\ \vdots & \vdots & & \vdots \\ \mathbf{0} & \mathbf{0} & \cdots & I_{n_u\times n_u} \end{bmatrix}_{m\times m}$$

$$L = \begin{bmatrix} I_{n_u\times n_u} & \mathbf{0} & \cdots & \mathbf{0} \\ I_{n_u\times n_u} & I_{n_u\times n_u} & \cdots & \mathbf{0} \\ \vdots & \vdots & & \vdots \\ I_{n_u\times n_u} & I_{n_u\times n_u} & \cdots & I_{n_u\times n_u} \end{bmatrix}_{m\times m}$$

$$b\,(k+1\,|k\,) = \begin{bmatrix} -\Delta u_{\max}\,(k) \\ \vdots \\ -\Delta u_{\max}\,(k+m-1) \\ \Delta u_{\min}\,(k) \\ \vdots \\ \Delta u_{\min}\,(k+m-1) \\ u\,(k-1) - u_{\max}\,(k) \\ \vdots \\ u\,(k-1) - u_{\max}\,(k+m-1) \\ u_{\min}\,(k) - u\,(k-1) \\ \vdots \\ u_{\min}\,(k+m-1) - u\,(k-1) \\ Y_p\,(k+1\,|k\,) - Y_{\max}\,(k+1) \\ -Y_p\,(k+1\,|k\,) + Y_{\min}\,(k+1) \end{bmatrix}_{(4m+2p)\times 1}$$

REFERENCES

[1] J. Zhao, "Chassis integrated control for active suspension, active front steering and direct yaw moment systems using hierarchical strategy," *Veh. Syst. Dyn.*, vol. 55, no. 1, pp. 72–103, 2017.

[2] J. Zhao, P. K. Wong, Z. Xie, X. Ma, and X. Hua, "Design and control of an automotive variable hydraulic damper using cuckoo search optimized PID method," *Int. J. Automot. Technol.*, vol. 20, p. 20, Feb. 2019, doi: 10.1007/s12239-018.

[3] X. Ma, P. Wong, J. Zhao, and Z. Xie, "Cornering stability control for vehicles with active front steering system using T-S fuzzy based sliding mode control strategy," *Mech. Syst. Signal Process.*, to be published, doi: 10.1016/j.ymssp.2018.05.059.

[4] J. Zhao, P. K. Wong, Z. Xie, C. Wei, and F. He, "Integrated variable speed-fuzzy PWM control for ride height adjustment of active air suspension systems," in *Proc. Amer. Control Conf. (Acc)*, Jul. 2015, pp. 5700–5705.

[5] X. Sun, C. Yuan, Y. Cai, S. Wang, and L. Chen, "Model predictive control of an air suspension system with damping multi-mode switching damper based on hybrid model," *Mech. Syst. Signal Process.*, vol. 94, pp. 94–110, Sep. 2017.

[6] X. Xu, W. Wang, N. Zou, L. Chen, and X. Cui, "A comparative study of sensor fault diagnosis methods based on observer for ECAS system," *Mech. Syst. Signal Process.*, vol. 87, pp. 169–183, Mar. 2017.

[7] H. Kim, H. Lee, and H. Kim, "Asynchronous and synchronous load leveling compensation algorithm in airspring suspension," in *Proc. Int. Conf. Control, Autom. Syst.*, vols. 1–6, Oct. 2007, pp. 2262–2267.

[8] I. Jang, H. Kim, H. Lee, and S. Han, "Height control and failsafe algorithm for closed loop air suspension control system," in *Proc. Int. Conf. Control, Autom. Syst.*, vols. 1–6, Oct. 2007, pp. 373–378.

[9] D. Ha, H. Kim, and H. Lee, "Height sensor fault diagnosis for electronic air suspension (EAS) system," in *Proc. IEEE Int. Symp. Ind. Electron.*, Jul. 2009, pp. 211–216.

[10] H. Kim and H. Lee, "Height and leveling control of automotive air suspension system using sliding mode approach," *IEEE Trans. Veh. Technol.*, vol. 60, no. 5, pp. 2027–2041, Jun. 2011.

[11] Y. Qin, F. Zhao, Z. Wang, L. Gu, and M. Dong, "Comprehensive analysis for influence of controllable damper time delay on semi-active suspension control strategies," *J. Vib. Acoust.*, vol. 139, no. 3, pp. 031006, 2017.

[12] Y. Qin, C. Xiang, Z. F. Wang, and M. Dong "Road excitation classification for semi-active suspension system based on system response," *J. Vib. Control*, vol. 24, no. 13, pp. 2732–2748, 2018.
[13] X. Ma, P. K. Wong, and J. Zhao, "Practical multi-objective control for automotive semi-active suspension system with nonlinear hydraulic adjustable damper," *Mech. Syst. Signal Process.*, vol. 117, pp. 667–688, Feb. 2018.
[14] J. Zhao, P. K. Wong, Z. C. Xie, C. Y. Wei, and R. C. Zhao, "Design and evaluation of a ride comfort based suspension system using an optimal stiffness-determination method," *Trans. Can. Soc. Mech. Eng.*, vol. 40, no. 5, pp. 773–785, 2016.
[15] J. Zhao, P. Wong, Z. Xie, X. Ma, and C. Wei, "Design of a road friendly SAS system for heavy-duty vehicles based on a fuzzy-hybrid-ADD and GH-control strategy," *Shock Vib.*, vol. 2016, Sep. 2016, Art. no. 6321765, doi: 10.1155/2016/6321765.
[16] J. Zhao, P. K. Wong, Z. C. Xie, and X. B. Ma, "Cuckoo search-based intelligent control of a novel variable rotary valve system for engines using PID controller," *J. Intell. Fuzzy Syst.*, vol. 32, no. 3, pp. 2351–2363, 2017.
[17] Z. Xie, P. K. Wong, J. Zhao, T. Xu, K. I. Wong, and H. C. Wong, "A noise-insensitive semi-active air suspension for heavy-duty vehicles with an integrated fuzzy-wheelbase preview control," *Math. Problems Eng.*, vol. 2013, Jun. 2013, Art. no. 121953, doi: 10.1155/2013/121953.
[18] L. Khan, S. Qamar, and U. Khan, "Adaptive PID control scheme for full car suspension control," *J. Chinese Inst. Eng.*, vol. 39, no. 2, pp. 169–185, 2016.
[19] Y. Qin, C. Wei, X. Tang, N. Zhang, M. Dong, and C. Hu, "A novel nonlinear road profile classification approach for controllable suspension system: Simulation and experimental validation," *Mech. Syst. Signal Process.*, to be published, doi: 10.1016/j.ymssp.2018.07.015.
[20] J. Zhao, P. K. Wong, X. Ma, and Z. Xie, "Design and analysis of an integrated SMC-TPWP strategy for a semi-active air suspension with stepper motor-driven GFASA," *Proc. Inst. Mech. Eng., I, J. Syst. Control Eng.*, vol. 232, no. 9, pp. 1194–1211, 2018.
[21] M. Taghizadeh, F. Najafi, and A. Ghaffari, "Multimodel PD-control of a pneumatic actuator under variable loads," *Int. J. Adv. Manuf. Technol.*, vol. 48, nos. 5–8, pp. 655–662, 2010.
[22] T. Yoshimura, A. Kume, M. Kurimoto, and J. Hino, "Construction of an active suspension system of a quarter car model using the concept of slicing mode control," *J. Sound Vib.*, vol. 239, no. 2, pp. 187–199, 2001.
[23] R. C. Zhao, P. K. Wong, Z. C. Xie, and J. Zhao, "Real-time weighted multi-objective model predictive controller for adaptive cruise control systems," *Int. J. Automot. Technol.*, vol. 18, no. 2, pp. 279–292, 2017.
[24] D. Shi, T. Liu, Q. Wang, and Q. Lan, "Vibration analysis of arbitrary straight-sided quadrilateral plates using a simple first-order shear deformation theory," *Results Phys.*, vol. 11, pp. 201–211, Dec. 2018.
[25] D. Q. Mayne, J. B. Rawlings, C. V. Rao, and P. O. M. Scokaert, "Constrained model predictive control: Stability and optimality," *Automatica*, vol. 36, no. 6, pp. 789–814, 2000.
[26] S. J. Qin and T. A. Badgwell, "A survey of industrial model predictive control technology," *Control Eng. Pract.*, vol. 11, no. 7, pp. 733–764, 2003.
[27] J.-H. Zhong, P. K. Wong, and Z. X. Yang, "Fault diagnosis of rotating machinery based on multiple probabilistic classifiers," *Mech. Syst. Signal Process.*, vol. 108, pp. 99–114, Aug. 2018.
[28] P. K. Wong, Z. C. Xie, J. Zhao, T. Xu, and F. He, "Analysis of automotive rolling lobe air spring under alternative factors with finite element model," *J. Mech. Sci. Technol.*, vol. 28, no. 12, pp. 5069–5081, 2014.
[29] F. Chang and Z.-H. Lu, "Dynamic model of an air spring and integration into a vehicle dynamics model," *Proc. Inst. Mech. Eng., D, J. Automobile Eng.*, vol. 222, no. 10, pp. 1813–1825, 2008.
[30] H. Zhang, D. Shi, S. Zha, and Q. Wang, "Sound-vibration behaviors of the thin orthotropic rectangular fluid–structure coupled system resting on varying elastic Winkler and Pasternak foundations," *Results Phys.*, vol. 11, pp. 188–200, Dec. 2018.
[31] M. K. Balki, C. Sayin, and M. Canakci, "The effect of different alcohol fuels on the performance, emission and combustion characteristics of a gasoline engine," *Fuel*, vol. 115, pp. 901–906, Jan. 2014.
[32] M. Z. Q. Chen, Y. Hu, C. Li, and G. Chen, "Performance benefits of using inerter in semiactive suspensions," *IEEE Trans. Control Syst. Technol.*, vol. 23, no. 4, pp. 1571–1577, Jul. 2015.
[33] Y. Qin, Z. Wang, C. Xiang, E. Hashemi, A. Khajepour, and Y. Huang, "Speed independent road classification strategy based on vehicle response: Theory and experimental validation," *Mech. Syst. Signal Process.*, vol. 117, pp. 653–666, Feb. 2019.
[34] Y. Qin, Z. Wang, C. Xiang, M. Dong, C. Hu, and R. Wang, "A novel global sensitivity analysis on the observation accuracy of the coupled vehicle model," *Vehicle Syst. Dyn.* to be published, doi: 10.1080/00423114.2018.1517219.
[35] D. Q. Mayne, "Model predictive control: Recent developments and future promise," *Automatica*, vol. 50, no. 12, pp. 2967–2986, 2014.
[36] X. Ma, P. K. Wong, and J. Zhao, "Adaptive regulating of automotive mono-tube hydraulic adjustable dampers using gray neural network–based compensation system," *Proc. Inst. Mech. Eng., D, J. Automobile Eng.*, to be published, doi: 10.1177/0954407018800580.
[37] S. H. Mathisen, T. I. Fossen, and T. A. Johansen, "Non-linear model predictive control for guidance of a fixed-wing UAV in precision deep stall landing," in *Proc. Int. Conf. Unmanned Aircraft Syst.*, Jun. 2015, pp. 356–365.
[38] L. Deori, S. Garatti, and M. Prandini, "A model predictive control approach to aircraft motion control," in *Proc. Amer. Control Conf.*, Jul. 2015, pp. 2299–2304.

XINBO MA received the Ph.D. degree from the Department of Electromechanical Engineering, University of Macau, in 2018.

She is currently with the Automotive Engineering Laboratory, Department of Electromechanical Engineering, University of Macau. Her research interests include automotive engineering, vehicle dynamics and control, and mechanism and machine theory.

PAK KIN WONG received the Ph.D. degree in mechanical engineering from The Hong Kong Polytechnic University, Hong Kong, in 1997.

He is currently a Professor with the Department of Electromechanical Engineering and the Associate Dean (Academic Affairs) of the Faculty of Science and Technology, University of Macau. He has published over 214 scientific papers in refereed journals, book chapters, and conference proceedings. His research interests include automotive engineering, fluid transmission and control, artificial intelligence, and mechanical vibration.

JING ZHAO received the Ph.D. degree from the Department of Electromechanical Engineering, University of Macau, in 2016. He is currently with the Automotive Engineering Laboratory, Department of Electromechanical Engineering, University of Macau. He has authored/co-authored over 50 papers in refereed journals and conference proceedings. His research interests include vehicle dynamics and control, mechanism and machine theory, fluid mechanics, and finite-element analysis.

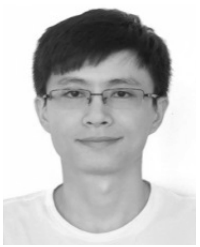

JIAN-HUA ZHONG received the M.S. and Ph.D. degrees in electromechanical engineering from the University of Macau in 2011 and 2016, respectively.

He is currently an Assistant Professor with the School of Mechanical Engineering and Automation, Fuzhou University, China. He has published over 20 papers in refereed journals and conference proceedings. His research interests include rotating machinery condition monitoring, vehicle dynamics and control, signal processing, pattern recognition, and fault diagnosis using machine learning methods.

HUANG YING received the B.S. degree in measurement and control technology and instrument from the Chengdu University of Technology in 2013 and the M.S. degree in electromechanical engineering from the University of Macau in 2018.

Her research interests include the modeling of active air suspension for vehicle, model predictive control, and application to automotive active air suspension systems.

XING XU received the B.S. degree in automotive engineering, the M.S. degree in control theory and control engineering, and the Ph.D. degree in agricultural electrification and automation from Jiangsu University, Zhenjiang, China, in 2002, 2006, and 2010, respectively.

He is currently a Professor with the School of Automotive and Traffic Engineering, Jiangsu University, China. He has published over 30 scientific papers in refereed journals, book chapters, and conference proceedings. His research interests include automotive engineering, vehicle dynamics and control, signal processing, and fault diagnosis.